Photochemical transformation of residential wood combustion emissions: dependence of organic aerosol composition on OH exposure

Anni Hartikainen[1], Petri Tiitta[1], Mika Ihalainen[1], Pasi Yli-Pirilä[1], Jürgen Orasche[2], Hendryk Czech[1,2,3] Miika Kortelainen[1], Heikki Lamberg[1], Heikki Suhonen[1], Hanna Koponen[1], Liqing Hao[4], Ralf Zimmermann[2,3], Jorma Jokiniemi[1], Jarkko Tissari[1], and Olli Sippula[1,5]

[1] Department of Environmental and Biological Sciences, University of Eastern Finland, Kuopio, FI-70211, Finland
[2] Joint Mass Spectrometry Centre, Comprehensive Molecular Analytics, Helmholtz Zentrum München, Neuherberg, DE-85764, Germany
[3] Joint Mass Spectrometry Centre, Institute of Chemistry, University of Rostock, Rostock, DE-18059, Germany
[4] Department of Applied Physics, University of Eastern Finland, Kuopio, FI-70211, Finland
[5] Department of Chemistry, University of Eastern Finland, Joensuu, FI-80101, Finland

Correspondence to: Anni Hartikainen (anni.hartikainen@uef.fi)

Abstract. Residential wood combustion (RWC) emits large amounts of gaseous and particulate organic aerosol (OA). In the atmosphere, the emission is transformed via oxidative reactions, which are under daylight conditions driven mainly by hydroxyl radicals (OH). This continuing oxidative aging produces secondary OA and may change the health- and climate-related properties of the emission. However, it is not well known how the composition of RWC-originated OA changes as the function of OH-exposure. In this work, emissions from two modern residential logwood combustion appliances were photochemically aged in an oxidation flow reactor (PEAR OFR) with various OH exposure levels, reaching up to 6×10^{11} s cm^{-3} (equivalent to one week in the atmosphere). Gaseous organic compounds were analysed by proton transfer reaction time-of-flight mass spectrometry (PTR-ToF-MS), while particulate OA was analysed online by an aerosol mass spectrometer (SP-HR-ToF-AMS) and offline by thermal-optical analysis and thermal desorption-gas chromatography mass spectrometry~~.~~ (IDTD-GC-ToFMS). Photochemical reactions increased the mass of particulate organic carbon by a factor of 1.3–3.9. The increase in mass took place during the first atmospheric equivalent day of aging, after which the enhancement was independent of the extent of photochemical exposure. However, aging increased the oxidation state of the particulate OA linearly throughout the assessed range, with ΔH:C/ΔO:C slopes between -0.17 and -0.49 in van Krevelen space. Aging led to an increase in acidic fragmentation products in both phases~~.~~, as measured by the IDTD-GC-ToFMS for the particulate and PTR-ToF-MS for the gaseous phase. For the ~~volatile~~gaseous organic compounds~~ measured by PTR-ToF-MS~~, the formation of small carbonylic compounds combined with the rapid degradation of primary volatile organic compounds such as aromatic compounds led to a continuous increase in both the O:C and H:C ratios. Overall, the share of polycyclic aromatic compounds (PACs) in particles degraded rapidly during aging, although some oxygen-substituted PACs, most notably naphthaldehydic acid, increased, in particular during relatively short exposures. Similarly, the concentrations of particulate nitrophenols rose extensively during the first atmospheric equivalent day. During continuous photochemical aging, the dominant ~~reaction~~transformation mechanisms shifted from the initial gas phase functionalisation/condensation to the transformation of the particulate OA by further oxidation reactions and fragmentation. The observed continuous transformation of OA composition throughout a broad range of OH exposures indicates that the entire atmospheric lifetime of the emission~~, from fresh to shortly aged to long~~

term aged emission (representative of long-range transported pollutants), needs to be explored to fully assess the potential climate and health effects of OARWC emissions.

1 Introduction

Biomass combustion is a major source of atmospheric particulate matter (PM) and is considered the main anthropogenic source of organic matter and the third largest contributor of black carbon (BC) emissions globally (Klimont et al., 2017). The use of wood fuels in small-scale residential settings is a main source for ambient organic aerosol (OA) in many parts of the world. For example, residential wood combustion (RWC) has been identified as a major source of ambient air fine particles in several European cities, where its relative contribution has been estimated to further increase in the future while PM emissions from other sources, such as industry and traffic, are decreasing (Denier Van Der Gon et al., 2015; Klimont et al., 2017). The amount and contents of the RWC emissions depend greatly on combustion conditions which are generally affected by the combustion procedure, fuel, and appliance technology (Bhattu et al., 2019; Nuutinen et al., 2014; Orasche et al., 2013; Tissari et al., 2009). In logwood-fired appliances, there is also a strong variation in the emissions during the different combustion phases of batches, with ignition producing the highest organic emissions (Bhattu et al., 2019; Kortelainen et al., 2018). However, highest black carbon concentrations are emitted during the flaming phase, while the char burnout phase typically emits large amounts of carbon monoxide but low, mainly inorganic particulate emissions (Kortelainen et al., 2018). Combustion conditions also affect the emissions of many toxic compounds, such as polycyclic aromatic compounds (PACs) (Kim et al., 2013; Orasche et al., 2013), and are consequently strongly linked with the adverse health effects of the emissions (Bølling et al., 2009; Kanashova et al., 2018; Kasurinen et al., 2018).

Many of the main organic species in fresh, unagednot atmospherically aged wood smoke are connected to the composition of wood fuel, such as levoglucosan, a common biomass burning marker, and lignin degradation products such as methoxyphenols and their derivatives (Elsasser et al., 2013; McDonald et al., 2000; Orasche et al., 2013). In addition, the gaseous organic emission from RWC contains of hundreds of volatile organic speciesgaseous compounds (OGC) (Bhattu et al., 2019; Bruns et al., 2017; Hartikainen et al., 2018; Hatch et al., 2017; McDonald et al., 2000).), majority of which can be classified as volatile organic compounds (VOC) (Hatch et al. 2017), meaning that under ambient conditions they exist purely in gaseous phase. Notably, RWC is an important anthropogenic source for volatile organic compounds (VOCs)OGCs with high potential for secondary particulate organic aerosol (SOA) formation. The most potent SOA-precursor compounds include aromatic hydrocarbons and oxygenated species, such as phenolic and furanoic compounds (Bruns et al., 2016; Hartikainen et al.,2016; Hartikainen et al., 2018) and removal of these compounds either via improved combustion conditions or for example catalytic cleaning have been shown to be efficient in lowering the SOA potential of RWC emissions (Czech et al., 2017; Pieber et al., 2018). Furthermore, the gaseous emissions contain high amounts of carbonyls, such as formaldehyde and acetaldehyde, with adverse health effects (Reda et al., 2015; U. S. EPA).

OA has an atmospheric lifetime of approximately one week (Hodzic et al., 2016), during which its chemical composition and potential environmental and health effects are likely to transform extensively. In daylight conditions, hydroxyl radicals (OH) dominate this aging process, where the oxidation of VOCs and semi-VOCsOGCs forms a variety of functionalized products with lower vapour pressures. These. Some of these oxidised secondary organic species partition into the particulate phase, resulting in an enhancement of ambient air particulate organic matter concentrations (Robinson et al., 2007). While aromatic VOCscompounds are noted as the main SOA precursors from RWC, the complete pathway

for SOA formation and the final SOA yields of complex ~~VOC~~OGC mixtures under different atmospheric conditions remain unclear (Bruns et al., 2016; Hartikainen et al., 2018; Hatch et al., 2017; McFiggans et al., 2019). Recent experiments on RWC exhaust estimate the mass of particulate OA to increase by a factor of 1.6–5.3 within approximately one day of photochemical aging (Bertrand et al., 2017; Bruns et al., ~~2015~~2015b; Grieshop et al., 2009; Heringa et al., 2011; Tiitta et al., 2016). In addition, ~~the photochemical transformation~~heterogeneous oxidation reactions of the particulate matter may be significant ~~when considering~~during the atmospheric ~~fate~~transformation of RWC emissions: it has been reported that only a minority of initial biomass burning particulate OA remains unreacted after a few hours of atmospheric aging (Hennigan et al., 2011; Tiitta et al., 2016). Photochemical aging also decomposes hydrocarbonaceous PACs (i.e., polycyclic aromatic hydrocarbons ~~(;~ PAHs~~) in both the particulate and the gas phase,~~), which ~~may decrease the~~cause adverse health effects due to their carcinogenic properties ~~of the emissions or on~~. On the other hand, atmospheric aging may lead to ~~the~~ formation of even more toxic, oxygen- or nitrogen-substituted PACs (Keyte et al., 2013; Miersch et al., 2019). For instance, these substituted PACs have been reported to cause a substantial part of the particle-induced mutagenicity in Beijing, with a contribution of only 8 % relative to the concentration of hydrocarbon PACs (Wang et al., 2011). Similarly, oxidation in nitrogen oxide (NO_x)-rich conditions can produce nitrophenols which are known to be harmful to ~~toward~~ plant growth and ~~for~~ human health (Harrison et al., 2005) and have been identified as an important constituent of light-absorbing organic matter ('brown carbon') (Moise et al., 2015; Zhang et al., 2011), thereby affecting atmospheric radiative forcing.

The photochemical aging of RWC emissions has previously been studied in smog chambers (Bertrand et al., 2017; Bruns et al., ~~2015~~2015a-b; Heringa et al., 2011; Tiitta et al., 2016), where the aging was monitored as a batch process from fresh emission to up to one atmospheric equivalent day of exposure (eqv.d) assuming an ambient average OH concentration of 10^6 molec cm^{-3}; Prinn et al., 2001). As an alternative, oxidation flow reactors (OFRs) with continuous sample flow have been increasingly utilised in combustion emission studies~~.~~ (Bruns et al., 2015a; Czech et al., 2017; Pieber et al., 2018). To achieve similar or higher oxidant exposures than chambers in shorter residence times, OFRs have been used with high ozone concentrations together with high-intensity low-wavelength UV lamps to generate OH-radical concentrations orders of magnitudes higher than those of smog chambers (Kang et al., 2007; Ihalainen et al., 2019; Simonen et al., 2017). Thus, OFRs enable measurements with better temporal resolution, which is a benefit when assessing the aging of aerosols from dynamic sources, such as batchwise logwood combustion.

In this study, we ~~investigated~~aim to determine how atmospheric aging changes the ~~photochemical transformation~~composition of organic aerosol, emitted by logwood fired stoves, as the ~~OA~~ function of OH-exposure. The atmospheric transformation of emissions from two RWC appliances fired with spruce and beech logwood~~. Atmospheric aging~~ was simulated using the photochemical emission aging flow tube reactor (PEAR~~) (~~ OFR; Ihalainen et al., 2019~~). In the PEAR, emissions were exposed~~) at different exposure levels ranging up to a ~~range of OH concentrations, after which the~~week of atmospheric age. The transformation of emissions and the formation of related secondary organic emissions were ~~measured~~monitored with a comprehensive ~~analysis~~ setup (Fig. 1~~). The OA measurements included~~), including analysis of gas-phase~~ analysis~~ by proton transfer reactor time-of-flight mass spectrometry (PTR-ToF-MS) and investigation of the particulate phase online by aerosol mass spectrometry (SP-HR-ToF-AMS) and offline by targeted gas chromatography mass spectrometry and thermal-optical analyses. ~~With photochemical exposure varying from 0 to 7 eqv.d, we assessed~~Together, these analyses enable the ~~transformation~~assessment of the OA chemical composition in both bulk and molecular level, from fresh emission to up to exposures representative of long-range transported smoke.

2 Material and methods

2.1 Experimental conditions

Experiments were conducted in the ILMARI laboratory of the University of Eastern Finland (www.uef.fi/ilmari) with the experimental setup shown in Figure 1. The two combustion appliances used were modern stoves with improved air intakes. First, a heat-storing masonry heater (Hiisi 4, Tulikivi Ltd., Finland) representing the typical modern logwood combustion technology utilised in Northern Europe, was fired with spruce logwood. The combustion procedure in the masonry heater consisted of three 2.5-kg batches (35-min combustion time) of spruce logwood representing kiln-dried fuel (5 % moisture content, S-5%), after which there was a 25-min char burning period prior to two 45-min batches with moist (22 % moisture content, S-22%) spruce logwood. Second, a non-heat retaining chimney stove (Aduro 9.3, Denmark) representing Middle-European modern logwood stoves was fired with both beech and spruce logs. The chimney stove experiments consisted of five 2-kg batches (combustion time 40–55 min) of beech logwood (17% H_2O, B-17%), followed by two 50-min batches of S-22%. Beech was used in these experiments because it is the most common firewood used in Middle Europe, while spruce is used both in Northern and Middle Europe. For ignition, 150 g of dry kindling was placed on the top of the first batch in the cold furnace. Each batch was divided into three parts: ignition, flaming, and burnout phase. The ignition phase was determined to last from the beginning of the batch to the moment of batch maximum flue gas CO_2 concentration, and the burnout phase to begin from the moment when the CO concentration started to elevate and remained at a high level until the end of the batch (Fig. 2). The modified combustion efficiency (MCE) as a function of time was calculated from primary flue-gas CO_2 and CO concentrations as $\Delta CO_2 / (\Delta CO_2 + \Delta CO)$.

The exhaust was sampled from the stack with a 10 µm pre-cut cyclone. The sample was diluted with a combination of a porous tube diluter and an ejector diluter (Dekati FPS ejector, Finland) and had a dilution ratio (DR) of 40–150 (Table 1) when fed to the PEAR OFR. In the chimney stove experiments, an additional ejector diluter with a DR of 8 (Dekati DI-1000, Finland) was placed before the secondary online aerosol instruments. Compared to the no-aging experiments, a higher DR was selected for the aging experiments in response to the expected increase in particulate matter in the PEAR OFR during photochemical aging. Measured concentrations were corrected for the dilution and normalised to stoichiometric dry flue-gas by multiplication with the stoichiometric correction factor (SCF) of Eq. 1 based on the ~~secondary~~background CO_2 concentration ($CO_{2,bg}$), the CO_2 concentration in the diluted sample downstream the PEAR OFR ($CO_{2,sec}$), and the fact that the dry flue gas of wood combustion with no excess air contains 20.2 % CO_2.

$$SCF = \frac{20.2\,\% - CO_{2,background}}{CO_{2} - CO_{2,background}} \frac{20.2\,\% - CO_{2,bg}}{CO_{2,sec} - CO_{2,bg}} \quad (1)$$

In addition, the secondary concentrations were normalised to a 13 % flue-gas oxygen content.

2.2 Use of the PEAR OFR

The PEAR OFR (Ihalainen et al., 2019) was used to continuously age the sample stream. In the setup, the extent of photon flux and consequential photochemical aging were controlled by adjusting the voltage of the 254-nm UV lamps. The total flow through the PEAR OFR was 60 L~~/~~ min~~-~~$^{-1}$ and the residence time within the PEAR 139 s . In addition to the 55 L~~/~~ min^{-1} sample flow, ~~additional~~ humified and purified air was introduced to the PEAR OFR to obtain a relative humidity of 45 ± 5 %. ~~In the aging experiments, 0.25–0.5 L/min ozone and 15 mL/min of butanol-*d9* were mixed with the main sample flow before the PEAR inlet (Fig. 1).~~ In the PEAR OFR, the photolysis of the ozone ~~formed~~forms hydroxyl radicals via reactions (2) and (3). Thus, the extent of photochemical aging in the PEAR ~~depended~~OFR depends on the photon flux inside the reactor and the introduction of OH precursors, namely, the externally fed O_3 and H_2O vapours.

$$O_3 + h\nu \rightarrow O_2 + O(^1D) \quad (2)$$

$$O(^1D) + H_2O \rightarrow 2\ \mathrm{OH} \quad (3)$$

In the aging experiments, ozone and butanol-d9 mixed with the main sample flow before the reactor inlet (Fig. 1) resulted in concentrations of 2-11 ppm of O_3 (Table 1) and 80-200 ppb of butanol-d9 in the PEAR OFR before initiation of photochemical aging. The OH exposure (OH_{exp}) was determined continuously based on the butanol-d9 concentrations downstream the PEAR according to the method presented by Barmet et al. (2012~~) by introducing a constant flow of butanol-*d9* to the PEAR.~~). The OH_{exp} for clean air in the PEAR prior to the exhaust input ranged from 8.2×10^{10} to 1.6×10^{12} molec cm^{-3} s, which is equivalent to 1–18 days in an ambient atmosphere (eqv.d) with an estimated 24-hour average global OH concentration of 1×10^6 molec cm^{-3} (Prinn et al., 2005). The alternate reaction pathways in the PEAR OFR, namely, exposure to photolysis ($flux_{254nm,exp}$), excited ($O(^1D)_{exp}$), atomic oxygen ($O(^3P)_{exp}$), and ozone ($O_{3,exp}$), were assessed using the OFR exposure estimation equations of Peng et al. (2016) for OFRs with 254-nm lamps. Both the OH_{exp} and the alternate reaction pathways were affected by the external OH reactivity (OHR_{ext}) (Li et al., 2015) of the gases in the sample fed to the PEAR OFR. The OHR_{ext} was calculated with Eq. (4) from the concentrations (c_i) of the primary gaseous compounds (Table S1) and the butanol-d9 in the PEAR OFR, with their OH reaction rate constants k_i ~~(Table S1).~~

$$OHR_{ext} = \sum k_i c_i \quad (4)$$

Due to the differences in the emission concentrations during logwood combustion also the OHR_{ext}, and consequently OH_{exp}, vary also within a batch (Fig. S9). Average OHR_{ext} was in the range 130 – 1300 s^{-1} with the highest contributions from CO, NO, and unsaturated hydrocarbons (Fig. S5).

Particulate wall losses inside the PEAR OFR were minimised by conductive stainless-steel walls, laminar flow, and a relatively small surface-to-volume ratio (2.28 m^2:139 L) (Ihalainen et al., 2019). The particulate losses were estimated ~~by~~to be approximately 6 % based on the loss of elemental carbon (EC~~),~~) in the PEAR OFR, determined from the difference ~~between~~in the thermal-optical EC concentrations measured upstream and downstream of the ~~PEAR, whereas losses~~ reactor. The fate of the gaseous organic compounds capable of irreversible condensation under the present experimental conditions, i.e., low-volatility organic compounds (LVOC~~) were modelled~~), was estimated based on ~~the model of~~ Palm et al. (2016) by considering three possible depletion pathways: condensation onto particles, reactions with OH radicals, and condensation onto walls. To estimate the fraction of LVOC condensing onto particle phase, condensation sinks (Fig. ~~).~~S7) were calculated according to Lehtinen et al. (2003) using an average of the particle size distributions up- and downstream the PEAR OFR. See Section S2.2 for further information on LVOC fate estimation.

2.3 Offline filter sampling and analysis

PM_1 filter samples were collected on Teflon (PTFE, Pall Corporation, P/N R2PJO47) and quartz fibre (QF, Pall Corporation, Tissuquartz) filters simultaneously from primary and secondary exhaust at a 10 L~~/~~ min^{-1} flow rate, following the methodology presented by Sippula et al. (2009). A pre-impactor (Dekati PM-10 impactor) was used to separate the particles with aerodynamic diameters less than 1 µm (PM_1). For the masonry heater, samples were collected separately from the S-5% combustion (100-min collection time) and S-22% combustion (90-min collection time). From the chimney stove, two sample pairs were collected from the combustion of beech: full first two batches (85-min collection time), and fourth and fifth batches excluding the last 15 minutes (85-min collection time). The third chimney stove collection consisted of the combustion of two full batches of moist spruce (100-min collection time).

The Teflon filters were weighted before and after sample collection to determine the total PM_1 mass of the emission. The amount of organic (OC) and elemental carbon (EC) in PM_1 was determined from the QF filters by using a thermal-optical carbon analyser (Sunset Laboratory Inc.) following the protocol NIOSH5040 (NIOSH, 1999). In-situ derivatisation thermal desorption–gas chromatography–time-of-flight mass spectrometry (IDTD-GC-ToFMS) (Orasche et al., 2011), was applied ~~to the~~for targeted analysis of ~~semi-VOCs~~organic compounds in the particulate phase from the QF filters. Non-polar and polar compounds were identified and quantified using mixtures of ~~isotope~~isotopically labelled internal standards and calibration standards; see Supplementary Information Chapter S6 for further information of the analysis procedure. Majority of the targeted compounds can be classified as either semi- or intermediately volatile, meaning that under the present experimental conditions they can be partitioned into both gaseous and particulate phases.

2.4 Online ~~aerosol~~gas-phase measurements

Fourier transform infrared spectrometer (FTIR DX4000, Gasmet Technologies Inc.) was implemented on the stack to measure the amount of NO_x, CO_2, CO, and 27 ~~VOCs~~OGCs (Table S1) in the fresh exhaust. The measured primary ~~VOCs~~OGCs were grouped into four subgroups: alkanes, oxygenated compounds, and unsaturated and aromatic hydrocarbons. ~~After the PEAR, the~~The concentrations of CO_2, O_3, NO_x, and SO_2 were monitored at the outlet of the PEAR OFR with a trace-level single-gas analyzers (ABB CO_2 analyser, Siemens), and ~~organic gaseous compounds in the mass-to-charge (m/z) range of 40–180~~OGC were measured by PTR-ToF-MS (PTR-TOF 8000, Ionicon Analytik, Innsbruck, Austria), with H_3O^+ as the reagent ion and an electric field to gas number density ratio (E/N) of 130. Mass calibration was done with ~~-~~H_3O^+ (m/z 21.02) and 1,3-diiodobenzene (m/z 203.94), which was added as a calibrant for higher m/~~z~~z. The processing of the PTR-ToF-MS data was done in a manner similar to that of earlier work (Hartikainen et al., 2018). Reaction rates by Cappellin et al. (2012) were used when available; for other compounds, the reaction rate with H_3O^+ was assumed to be 2×10^9 cm^3 s^{-1} (Table S6).

2.5 Online particulate-phase measurements

Particle concentrations and mobility size distributions were monitored with scanning mobility particle sizers before (SMPS 3082, TSI, size range 14.6–661.2 nm) and after the PEAR OFR (SMPS 3080, TSI, size range 15.1–661.2 nm). An electrical low pressure impactor (ELPI 10 L~~/~~ min^{-1}, Dekati) measured the particle aerodynamic size distribution and the concentration of primary particles in the size range 18.6–5950 nm. The total particulate mass after PEAR OFR was measured with a tapered element oscillating microbalance monitor (TEOM, Model 1405, Thermo Scientific).

The composition of submicron particulate matter after PEAR OFR was measured by soot particle aerosol mass spectrometer (SP-HR-ToF-AMS, Aerodyne Research Inc). ~~The~~ The SP-HR-ToF-AMS dual vaporizer mode was used, with the combination of the thermal vaporizer (600 °C) and the continuous wave laser vaporizer (1064 nm) enabling the study of both nonrefractory (NR-PM) and refractory light-absorbing submicron aerosol particles (R-PM, e.g., refractory black carbon (rBC)) (Onasch et al., 2012). Standard mass-based calibrations were performed for the ionisation efficiency in the SP-HR-ToF-AMS using ammonium nitrate and Regal Black (Regal 400R Pigment Black, Cabot Corp.) particles (Jayne et al., 2000; Onasch et al., 2012). SP-HR-ToF-AMS was operated in V-mode from 12 to 555 m/z and the two vaporizer configurations were alternated every 120 s, including the particle time-of-flight (PTOF) mode (duration 20 s). The SP-HR-ToF-AMS data was analysed using the standard analysis tools SQUIRREL v1.62A and PIKA v1.22D adapted in Igor Pro 8 (Wavemetrics). The data was corrected by time-dependent background gas-phase CO_2 subtraction using the online HEPA filter measurement technique. The interactions of inorganic salts with pre-deposited carbon on the tungsten

vaporizer was corrected according to Pieber et al. (2016). The CO_2-AMS interference calibration value was 0.3 % of the NO_3 concentration determined by NO_3NH_4 calibration and corrected via the fragmentation table according to Pieber et al. (2016). Before correction, the relative effect of the interference on O:C ratio was typically under 1 % and 5 % at maximum. The applied relative ionisation efficiency (RIE) was 1.4, which agrees with the OA mass concentrations of biomass-burning emissions within the stated ±38 % uncertainty of AMS (Bahreini et al., 2009; Xu et al. 2018). The elemental analysis of the OA was conducted using the Improved-Ambient method (Canagaratna et al., 2015), and the average carbon oxidation state (OS_C) of the OA was estimated as $OS_C \approx 2 \times$ O:C - H:C (Kroll et al., 2011).

The SP-HR-ToF-AMS OA mass spectra was further examined by positive matrix factorisation (PMF) using the method described in Lanz et al. (2007) and Ulbrich et al. (2009). Similar method have been used previously for example for the assessment of RWC generated POA and SOA in a chamber (Bruns et al., 2015a; Tiitta et al., 2016) and in an OFR (Bruns et al., 2015a) or for time-resolved analysis of RWC OA emission constituents (Elsasser et al., 2013; Czech et al., 2016). The PMF Evaluation Tool v.3.05 was applied, and the standard data pre-treatment process was completed based on Ulbrich et al. (2009), including the application of minimum error criteria and down-weighting weak variables as well as m/z 44 (CO_2^+) and water-related peaks. The final four-factor PMF solution covered 98 % of the OA spectra (2.2 % residual). Additional factors did not increase the realistic physical meaning of the solution, while fewer factors were insufficient for a meaningful presentation of the data. The factor identification was confirmed by comparing the time series and mass spectra of each factor with external tracers (nitrate, sulphate, ammonium, chloride, PAH, CO_2^+, $C_2H_3O^+$, $C_4H_9^+$, and $C_2H_4O_2^+$). Furthermore, the factors were compared to logwood combustion mass spectra measured by Tiitta et al. (2016) from the aging of spruce logwood exhaust in a smog chamber. The agreement of spectra was denoted with both a coefficient of determination (R^2) and the angle between two mass spectra vectors (Kostenidou et al., 2009), where an angle less than 15° indicates a good agreement between two mass spectra.

The polycyclic aromatic hydrocarbons ~~(PAH)~~ and other ~~polycyclic aromatic compounds (~~PAC~~)~~ in the exhaust were analysed by using the PAC molecular ions as a proxy, following the P-MIP methodology presented by Herring et al. (2015). The base molecular ions $[M]^+$, their fragments ($[M\text{-}H]^+$ and $[M\text{-}2H]^+$) and isotopes (^2H, ^{13}C, $^{13}C_2$, ^{15}N, ^{17}O, and ^{18}O) were isolated and quantified using the SP-HR-ToF-AMS high-resolution analysis software tool (version 1.22D). The targeted ions included those previously connected with PACs (Herring et al., 2015) and compounds typically released from ~~residential wood combustion~~RWC (Avagyan et al., 2016; Bertrand et al., 2018; Bruns et al., ~~2015~~2015b; Czech et al., 2018; Miersch et al., 2019). The 61 PACs considered (Table S8) were separated into five subgroups: unsubstituted PAHs (UnSubPAHs), oxygenated ~~PAHs~~PACs (OPAHs), methylated ~~PAHs~~PACs (MPAH), nitrogen-substituted ~~PAHs~~PACs (NPAHs), and amino ~~PAHs~~-PACs (APAHs). See Supplementary Information Chapter S5 for further information on SP-HR-ToF-AMS analyses.

3 Results and ~~conclusions~~discussion

This study comprehensively characterises the chemical properties of RWC exhaust at different atmospheric aging times by combining extensive information gathered from gas-phase and particulate phase chemical analyses. In this section, we first discuss the dynamic combustion conditions and the characteristics of primary emissions from logwood stoves utilized with different fuels, which define the starting point for the aging experiments. Next, the aging conditions in the PEAR OFR are evaluated in order to validate the atmospheric relevance of the results. Finally, we assess the changes in the gaseous and particulate OA during the aging process under a variety of different oxidant concentrations. The observations of changes both in bulk- and molecular level aerosol chemical composition demonstrate that the major transformation

pathway of OA changes from initial gas phase functionalisation followed by condensation to the transformation of the particulate OA by heterogeneous oxidation reactions and fragmentation. The study shows a linear dependency between OH exposure and organic aerosol oxidation state. Furthermore, OH-exposure-dependencies of specific OA constituents, such as nitrophenols, carboxylic acids and PACs, are established.

3.1 Combustion conditions

The average modified combustion efficiency was greater than 0.97 for the masonry heater and greater than 0.95 for the chimney stove, with lower MCE occurring mainly during the char burnout periods (Fig. S1). These values are typical for modern batch-wise operated logwood appliances (Bhattu et al., 2019; Czech et al., 2018; Heringa et al., 2011). In addition to the variation within a combustion batch, there were also differences between the individual batches (Fig. 2). Notably, the combustion conditions during the first batch were distinct from later batches~~. This was a result~~, because of the ~~lower initial temperature which~~ignition in a cold firebox. This caused a longer ignition period (determined by the rising CO_2 concentrations), which lasted for 24 ± 5 % (masonry heater) and 35 ± 4 % (chimney stove) of the total duration of the batch~~;~~, whereas in the later batches~~,~~ the firebox temperatures are higher ~~initial temperature shortened~~ and the ignition shortened to 9 ± 3 % (masonry heater) or 8 ± 4 % (chimney stove) of the total combustion time. Furthermore, the flaming phases of the first batches were shorter than those of the following batches of dry spruce or beech fuels. The emission profiles were affected by these batchwise differences, with ignition being the period for enhanced organic emissions, whereas the flaming phase was characterized by an increase in particulate emissions consisting mainly of black carbon, as expected based on previous work (Kortelainen et al., 2018). The char burnout phases with these fuels were characterised by high CO concentrations, whereas in moist spruce combustion elevated CO concentrations were measured throughout the batch, thus making the burnout phases less distinguishable.

3.2 Primary emissions

3.2.1 Gaseous organic emissions

The primary organic gaseous emissions in the undiluted flue gas were measured ~~constantly~~continuously by an FTIR multicomponent analyser~~ from the undiluted flue gas~~. Additionally, the PTR-ToF-MS measured diluted, unaged emissions during the no-aging experiments. These datasets complemented each other because, while FTIR ~~measured only~~ was calibrated for 27 typical combustion-derived ~~VOCs~~compounds (Table S1), a more detailed insight of the ~~VOC~~ composition of the gaseous organic phase was acquired via the PTR-ToF-MS~~ detection of 127~~, with which 126 different molecular formulas for ~~gaseous species~~OGC in the primary ~~aerosol~~emissions were identified in the m/z range of 40–180 (Table S6). However, PTR-ToF-MS is unable to detect ~~for example~~ compounds with proton affinities lower than that of water (691 kJ mol^{-1}), such as alkanes~~ because of their low protonation efficiency.~~. Furthermore, ~~the~~ fragmentation ~~of~~in the ~~-~~PTR-ToF-MS ~~limited in~~limits the ~~quantification~~identification of compounds with similar mass-to-charge ratios as ~~those of~~ common fragment ions, including unsaturated aliphatic compounds, such as propene ($C_3H_6^+$) at m/z 41.04 or butene ($C_4H_8^+$) at m/z 57.08~~; however~~. However, these compounds were detected ~~using~~by the FTIR.

The major ~~VOC~~OGC groups measured by PTR-ToF-MS were carbonyls, aromatic hydrocarbons~~,~~ (ArHC), furans, and phenols (Fig. ~~6~~4; Table S2). In addition, unsaturated aliphatic compounds constituted a substantial fraction of ~~VOC, as~~the total non-methane OGC (NM-OGC) measured using the FTIR (Fig. 3). The ~~total VOC~~NM-OGC emissions based on FTIR were 42.6 ± 9~~ ± 10.5~~.2 and ~~102 ± 28.0~~101 ± 24.6 mgC m^{-3} for dry and moist spruce combustion in the masonry heater, respectively, and 89.~~0 ± 13.5~~4 ± 11.3 and ~~147 ± 24.9~~148.3 ± 23.0 mgC m^{-3} for beech and moist spruce

in the chimney stove, respectively. Thus, the lowest ~~VOC~~NM-OGC concentrations were measured from the dry spruce combustion. Moist spruce combustion produced a factor of 1.7–3.6 higher emission than dry wood, which is well in line with studies by e.g. McDonald et al. (2000), where moist fuel produced 2–4 times more ~~VOC~~NM-OGC than dry fuel combustion. The difference between concentrations was highest for oxygenated compounds (factor of 4.2~~±~~ ± 1.7) and for unsaturated compounds (2.7±0.6), but statistically significant for all subgroups (paired t-test p-values ≤0.02 for all groups for the consecutive dry/moist experiments; Table S2). Differences in ~~VOC~~NM-OGC emissions were also observed between the masonry heater and the chimney stove. Emissions from moist spruce combusted in the chimney stove were higher by a factor of 1.5 (p-value 0.05) compared to the masonry heater, with a significant increase in unsaturated and aromatic hydrocarbons (factors of 1.6 and 1.7, respectively, p-values <0.01) based on FTIR measurements.

The ~~VOC~~NM-OGC emissions of the first batches exhibited a distinct time-dependent behaviour in comparison to the following batches~~; i.e.,~~: the emitted concentrations always increased both after ignition and at the end of flaming phase (Fig. 2), whereas in the following batches there was a sharp emission peak at ignition, after which the concentrations declined as soon as the flaming phase began. These findings agree with those by Kortelainen et al. (2018) and are influenced by the fact that cold ignition is performed from the top of a fuel batch, while the following batches are ignited from the bottom by the glowing embers. ~~VOC~~NM-OGC emissions were lowest during the burnout period when most of the fuel was already consumed (Fig. ~~S2~~2). Thus, ~~VOC~~NM-OGC emissions have a reverse time profile to the CO emissions, which peak during the char burnout phase. Furthermore, the contribution of the different organic compound groups to the total ~~VOC~~NM-OGC concentration differed in relation to time (Fig. ~~S3~~3, Fig. S2). For example, the importance of aromatic species increased for dry fuels (S-5% and B-17%) for the flaming and burnout phases, while other species were pronouncedly emitted at ignition. In addition, the composition of aromatic species measured with PTR-ToF-MS in the unaged emission depended on the phase (Fig. ~~S4~~S3). In the masonry heater, ~~aromatic hydrocarbons (~~ArHC~~)~~ had ~~a~~the highest contribution during the ignition phase, but their relative share decreased during flaming phase, while the share of furanoic and phenolic compounds increased. The relative importance of furanoic and phenolic compounds in the fresh exhaust of the flaming phase from a masonry heater has been also previously established (Czech et al. 2016). Overall, the share of ArHC in the fresh exhaust is higher and less phase-dependent for beech combustion in chimney stove than for other experiments. The share of N-containing aromatic compounds, namely, nitrophenol and -cresol, also increased after ignition. These findings are important also when considering the potential of SOA formation, as aromatic ~~VOCs~~compounds have been observed to be the major SOA precursors in RWC emissions, and removal of ArHC from the flue gas either by improving combustion conditions or using e.g. catalytic cleaning has been noted to decrease also the resulting SOA formation (Bruns et al., 2016; Hartikainen et al., 2018; Pieber et al., 2018).

3.2.2 Particulate emissions

The average primary PM_1 mass ~~emissions ranging from~~concentrations, 33 ~~to~~ – 67 mg m^{-3}, and the number ~~emissions from~~concentrations, 3.2×10^7 cm^{-3} ~~to~~ – 5.4×10^7 cm^{-3} (Table 2~~)~~), were on a similar level with earlier studies reporting emissions from modern logwood stoves (Kortelainen et al., 2018; Nuutinen et al., 2014; Tissari et al., 2009). The combustion of dry spruce in a masonry heater emitted 1.5- and 2 -fold PM_1 mass compared to that of moist spruce and beech, respectively, mainly because of the higher elemental carbon emissions. Moist spruce generated similar PM_1 emissions with both combustion appliances. The organic carbon to elemental carbon ratio (OC:EC) of dry spruce combustion was very low (0.07 ± 0.02, Table 2) compared to that of moist spruce combustion (0.31 ± 0.45 for masonry heater and 0.25 ± 0.04 for chimney stove) and beech combustion (0.15 ± 0.04). Such low OC:EC ratios have been

previously reported for emissions from modern masonry heaters operating with dry logwood (Czech et al., 2018; Miersch et al., 2019; Nuutinen et al., 2014).

The particle size distribution (~~Figs. 4 and S5~~Fig. S4) from dry spruce combustion was clearly distinguishable from that of other wood fuels and showed considerably larger mean particle mobility size (GMD 95.5 nm) compared to those of other fuels (GMD 52.8–68.4 nm). The soot-dominated composition of S-5% exhaust likely increases the GMD, because soot particles are typically present as larger agglomerates than particles of inorganic origin (ash) which mainly form ultrafine particles (Tissari et al., 2008). The size distribution and number concentration of particles in an exhaust are not only important because of their link to potential health effects, but also during aging of the exhaust, because they affect the condensation sink (CS) (Lehtinen et al., 2003) of condensable vapours during the dilution and aging process. Thus, the particle number concentrations and size distributions affect the fate of condensable vapours and the overall OA enhancement ratios. ~~The fates of low-volatility condensable vapours are further discussed in the chapter 3.3.1.~~

The thermal-optically measured elemental carbon in both the primary and the secondary exhausts correlated well with the refractory black carbon (rBC) measured by SP-HR-ToF-AMS from the secondary exhaust (R^2 = 0.74 and 0.76, respectively; see Fig. ~~S14~~S15). Analogous to the elemental carbon results, rBC emission was highest during the combustion of kiln-dried spruce (49.3 ± 13.7 mg m^{-3}). Dry fuel has recently been found to increase the soot and PAC emissions also for combustion of birch logwood in sauna stoves (Tissari et al., 2019). Considering the different combustion phases, rBC emissions were highest during high-temperature, flaming combustion as previously noted also by e.g. Kortelainen et al. (2018). For moist spruce, the rBC concentration dropped to 24.8 ± 12.3 mg m^{-3}, likely because of the lower temperature and consequentially slower burn rate. Similar rBC concentrations (24.0 ± 6.0 mg m^{-3}) were also measured from spruce combustion in the chimney stove. Unlike the masonry heater where the rBC concentrations were similar throughout the three dry batches, the rBC concentration from the combustion of beech in a chimney stove decreased considerably after the first batch, from 57.7 ± 7.2 mg m^{-3} to 15.6 ± 5.2 mg m^{-3}. While aging had no effect on the rBC mass, it plays an important role in the formation of SOA by acting as a seed for condensation during aging. Furthermore, soot cores composed of elemental carbon are chemically active and may enhance the photooxidation of an OA condensed onto soot agglomerates through electron transfer (Li et al., 2018).

3.3 OFR conditions

~~**3.3.1 Wall losses and fate of condensable vapours**~~

~~The loss of primary particles in the PEAR was estimated at 6 % based on the thermal–optical measurements of elemental carbon. When estimating the fate of the LVOC in the PEAR, three possible depletion pathways were considered: condensation onto particles, reactions with OH radicals, and condensation onto walls (Palm et al., 2016). To estimate the fraction of LVOC condensing onto particle phase, condensation sinks (Fig. 4) were calculated according to Lehtinen et al. (2003) using an average of the particle size distribution before and after PEAR. Similar to earlier studies, the downstream particle number concentration and condensation sinks were influenced by new particle formation (Fig. S13) with the extent of nucleation depending strongly on the aging conditions (Bruns et al., 2015; Ihalainen et al., 2019; Simonen et al., 2017). Long aging conditions greater than 4 eqv.d led to particularly strong increase in the amount of sub-50 nm particles. The new particle formation occurred mainly during the periods when the concentrations of condensable vapours were high; that is, most notably during the ignition phase. However, the distinct formation of ultrafine particles does not necessarily represent the atmospheric fate of condensable vapours because of the faster than ambient oxidation resulting in faster gas-to-particle conversion and higher saturation ratios in the PEAR. At lower OH exposures, the~~

~~condensation growth was mainly observed as an increase in the number concentration in the larger size range, while less nucleation to new particles was observed than that in long aging experiments.~~

~~The importance of different LVOC fates is shown in Figure 5. The majority of the LVOCs condensed onto the particles, and a portion also depleted by reactions with oxidants in the PEAR, while the LVOC wall losses were primarily below 2 %. The amount of LVOCs estimated to exit the PEAR as gas phase LVOCs exceeded 0.1 % only during the middle burnout phase of the masonry heater combustion because of the low particle number concentrations during the char burning phase between the change from dry spruce to moist spruce combustion, which generated a low condensation sink into the PEAR.~~

~~3.3.2 Photochemical aging conditions~~

During photochemical aging, ~~external OH reactivity (~~OHR_{ext}~~)~~ is an important parameter affecting OH-radical consumption and reaction pathways of organic species. For the masonry heater experiments, the average OHR_{ext} was ~~98–107~~130–150 s^{-1} for dry spruce samples and ~~125–172~~160–220 s^{-1} for moist spruce. In the chimney stove, the average OHR_{ext} was ~~237–252~~280–300 s^{-1} for beech and ~~278–308~~320–370 s^{-1} for moist spruce samples, except for the low-DR experiment (Exp. 5, DR of 30) where the average OHR_{ext} reached ~~684~~820 and ~~1110~~1300 s^{-1} for the beech and moist spruce samples, respectively. The OFR conditions were divided into good, risky, and bad based on the ratio of the photon flux exposure to OH_{exp} by the definitions of Peng and Jimenez (2017) (Fig. ~~S7~~S6). Here, the aging conditions were defined as mainly "risky" (4×10^5 cm s^{-1} < $flux_{254nm,exp}/OH_{exp}$ < 10^7 cm s^{-1}) during all the experiments. The OHR_{ext} varied considerably during combustion cycles, but the limit for ~~bad~~'bad' conditions was exceeded ~~briefly (up to 7 % of total experiment time)~~ only ~~in a few experiments~~ during ignition phases of chimney stove experiments when the OHR_{ext} peaks above 1000 s^{-1}~~.~~ for brief periods accounting for up to 4 % of total experiment time. In terms of OA emission, the ~~limit for bad conditions was exceeded in one masonry heater experiment (S-22%, Exp. 5), where 4 % of OA mass was emitted during this period. For the chimney stove experiments,~~ bad conditions accounted for ~~2–9~~3–7 % of chimney stove OA emissions, excluding the S-22% combustion for the low-DR experiment ~~(46~~where 30 % of OA was emitted under 'bad' conditions~~).~~.

~~The~~Evaluation of the OHR_{ext} ~~calculations were~~was limited to the externally added butanol-d9 and the compounds measured from the primary exhaust with FTIR, with NO, CO, and unsaturated hydrocarbons as the main OHR_{ext} producers (Fig. ~~S6~~S3). In other words, the products of later-generation oxidation or from fragmentation from the particulate phase were not considered. ~~In addition, the prevailing~~ The average NO_x concentrations input to the PEAR OFR ranged ~~on average~~ from 150 to 420 ppb, except for the low-DR experiment ~~at a concentration~~with concentrations of 1140 and 751 ppb for beech and spruce combustion, respectively. NO is rapidly oxidized to NO_2 with the addition of O_3 and then partially converted to particulate nitrate~~, and the~~. The subsequent low-NO conditions in the PEAR ~~reduced~~decreased the reactions of organic peroxy radicals (RO_2) with NO. Based on the RO_2 chemistry model by Peng et al. (2019) for 254 nm OFRs, the high photon fluxes and high concentrations of both OH and HO_2 in the PEAR OFR result in lower RO_2 lifetime and consequently lower RO_2 isomerization rate than in atmosphere, while the importance of RO_2+OH reaction is enhanced due to lower-than-ambient HO_2-to-OH-ratio (Peng et al. 2019).

The average batchwise OH exposure in the PEAR OFR during photochemical aging experiments ranged from 0.5 to 7 eqv.d depending on the applied photon flux and the OHR_{ext} of the sample. During the experiments, the photochemical exposure varied in line with the varying OHR_{ext} during batchwise combustion, with the highest exposure occurring during the flaming phase and lower exposure during the ignition period (Fig. ~~S8~~S9). The extent of alternative

non-OH reaction pathways during photochemical aging in the PEAR OFR were compared to the tropospheric conditions (Chapter S2.3), and the exposures to $O(^1D)$ and $O(^3P)$ in the PEAR OFR were ~~shown~~estimated to be similar to those in ambient conditions (Fig. ~~S9~~S10), excluding the ignition period during the low-DR experiment, where the importance of $O(^3P)_{exp}$ briefly exceeded ambient conditions. However, the exposure to ozone in relation to OH radicals was estimated to be lower in the PEAR OFR than in the troposphere ($O_{3,exp}/OH_{exp}<10^5$~~), thus leading to more OH-dominated chemical reactions when only considering the initial O_3 input.~~). However, our estimations were based on the initial O_3 concentrations, whereas O_3 is expected to form in the PEAR OFR during photochemical aging ~~because it is~~as a product of the OH + ~~VOC~~OGC reactions (Carter, 1994). This may have led to the $O_{3,exp}/OH_{exp}$ being slightly underestimated.

Several of the emitted ~~VOCs~~OGCs were susceptible to photolysis at 254 nm, most importantly the ~~aromatic hydrocarbons~~ArHC, which are among the main SOA precursors from RWC. Photolysis as a degradation pathway can exceed OH reactions also in the atmosphere for compounds with high photolysis rates (Hodzic et al., 2015). Here, the importance of photolysis was notable for e.g. benzene, of which more than 40 % may have degraded via photolysis (Fig. ~~S10~~S11). However, the importance of photolysis during photochemical aging is inversely proportional to the ratio of the OH reaction rate to the photoabsorption cross section (σ_{abs}), and it can be considered a minor pathway for other main ~~VOC species~~OGCs (Table S5), including other aromatic species such as toluene (<10 % of total degradation during these experiments~~, see~~; Fig. ~~S10).~~ S11).

The detailed results of the LVOC fate calculations are presented in the section S2.2. Briefly, the majority of LVOCs were estimated to condense into the particulate phase in all experimental conditions (Fig. S8). Similar to earlier OFR studies (Bruns et al., 2015a; Ihalainen et al., 2019; Simonen et al., 2017), the downstream particle number concentration and condensation sinks were influenced by new particle formation (Fig. S14) with the extent of nucleation depending strongly on the aging conditions and the concentrations of condensable vapours. However, the distinct formation of ultrafine particles does not necessarily represent the atmospheric fate of condensable vapours because of the faster-than-ambient oxidation, which results in higher saturation ratios and faster gas-to-particle conversion in the PEAR. Gas-to-particle conversion is also affected by the dilution ratio, which was in the PEAR OFR lower than what typically exists in atmosphere. Therefore, it has to be noted that the relative fraction of the measured semivolatile species in the condensed phase are likely lower at ambient dilution ratios than in the OFR experiments of this study.

3.4 Transformation of gaseous phase

The composition of the ~~VOCs~~OGCs changed throughout the studied exposure range, and the abundance of the secondary ~~VOCs~~compounds increased with an increase in photochemical exposure. However, while the small oxidised organics became increasingly dominant in the gas phase, photochemical aging particularly decreased the share of aromatic compounds (Fig. ~~6~~4). Namely, the ~~VOCs~~OGCs measured with PTR-ToF-MS from the aged gas phase were governed by small carbonyls and fragmentation products such as acetic acid ($C_2H_4O_2$, m/z 61.02). The evolution of the total chemical composition is visualised in the van Krevelen ~~-~~diagram, which is often used for simplified characterisation of particulate OA (Heald et al., 2010) and was here extended for the investigation of the gaseous organic phase measured by PTR-ToF-MS (Fig. ~~7~~5). Photochemical aging caused several simultaneous and subsequent functionalisation reactions of the organic compounds, and the increase in the average H:C ratio together with an increasing O:C ratio led to linear slopes from +0.69 to +1.0 in the van Krevelen diagram. Similar, positive slopes are derivable also from previous studies of aging of RWC OGC in smog chambers (Bruns et al., 2017; Hartikainen et al., 2018). Most of the ~~VOCs~~OGCs in primary RWC exhaust have relatively high OH reactivities (Fig. ~~S11~~S12), and thus their reactions are expected to take place within the first

atmosphere equivalent hours of photochemical aging (Bruns et al., 2017; Hartikainen et al., 2018). ~~This indicates the continuous contribution from~~Therefore the secondary OGC products, including the oxidised fragmentation products from the particulate phase, dominate the total OGC in the long-range transported smoke. In addition, the loss of compounds with low H:C and O:C ratios, such as aromatic species, is important for the change of the average composition. Furthermore, the oxidation of compounds undetected by the PTR-ToF-MS, such as alkanes, may introduce secondary products with higher proton affinities and their ~~consequent~~subsequent appearance in the spectra. Conversely, aging may also lead to the growth of compounds outside the ~~considered~~observable mass range (m/z 40–180). Compared to previously measured changes of RWC exhaust in a chamber (Hartikainen et al., 2018), aging in the PEAR OFR led to a slightly higher increase in the H:C ratio. This difference implies an increased fragmentation which is likely the result of faster ~~aging process~~OH exposure and differences in the RO_2 chemistry (Peng et al., 2019) in the PEAR OFR compared to that in a smog chamber.

Aromatic compounds consisting of ~~aromatic hydrocarbons (~~ArHCs~~),~~ phenols, furans, N-containing aromatic compounds (N-aromatics), and other oxygenated aromatics were important constituents of the primary organic gas phase and formed 37–39 % of the fresh ~~VOCs~~emission from the masonry heater and 33–34 % from the chimney stove, as measured by the PTR-MS-TOF (Fig. ~~9~~4). Similar shares have been measured from fresh RWC exhaust by Bruns et al. (2017) (13–33 %) and Hartikainen et al. (2018) (33 –36 %). However, after 2 eqv.d of exposure, their share decreased to less than 20 % of the identified ~~VOCs~~OGCs, which agrees with previously reported conversions of aromatics during photochemical exposure (Bruns et al., 2017; Hartikainen et al., 2018). Overall, the photochemical reactions of aromatics are an important source of SOA because they form products that efficiently partition into the particulate phase. However, there are large differences between the conversion efficiencies of aromatic compound groups. While ArHCs comprise approximately half of the aromatic ~~VOCs~~compounds in fresh gaseous exhaust, their share grows to over 70 % in 5–7 eqv.d, while the share of oxygenated aromatics decreases with aging in line with their higher OH reactivity. Similar aromatic behaviour in RWC exhaust was observed earlier in a chamber with spruce exhaust (Hartikainen et al., 2018), where the molar share of ArHCs in the total aromatic content increased from 45 % and 32 % to 63 % and 54 % during aging of 0.6 and 0.8 eqv.d, respectively, while the share of furanoic and phenolic species decreased. Furthermore, N-aromatics were not detectable here with ages exceeding 1 eqv.d, although they have been observed to form with shorter exposures (Hartikainen et al., 2018). The N-aromatics produced by the first stages of aging may have partitioned to the particulate phase but are also degraded by subsequent reactions with OH. Simultaneously, the share of aliphatic nitrogen compounds (CHN and CHNO) to the total concentration ~~remained relatively stable.~~was not substantially affected by photochemical exposure.

Carbonyls were divided into primary and secondary subgroups based on their behaviour during aging (Table S6). The primary carbonyl group, consisting mainly of acetaldehyde and to a smaller extent of compounds such as acrolein and butadiene, was prevalent in the fresh exhaust, but their share of identified compounds decreased from 13–27 % in unaged exhaust to 3–12 % in the highest exposures. This is the result of both the degradation of these compounds and the introduction of high amounts of carbonyls in the secondary carbonyl group. The ratio between the two carbonyl groups increased linearly with age (Fig. ~~S12~~S13). The secondary carbonyl group was dominated by acetic acid, which was the most prevalent compound after extensive aging in all experiments and covered over 30 % of the total measured ~~VOC~~OGC concentration from the highly aged S-5% and B-17% exhaust. The mainly small acidic compounds in the secondary carbonyl group were formed from the photochemical reactions of ~~VOCs~~OGCs and from particulate OA, which is a consistent source of oxygenated ~~VOCs~~OGCs such as acetic acid, formic acid, acetaldehyde, and acetone (Malecha and

Nizkorodov, 2016). Of these, acetaldehyde is classified as a primary carbonyl because it reacts with OH two orders of magnitude faster than the ~~others~~other considered small carbonyls (Atkinson et al., 2001), and thus its concentration remains ~~stable~~at a similar level throughout the aging process.

3.5 Transformation of particulate phase

3.5.1 OA enhancement and composition

The photochemical aging process increased the mass of particulate organic carbon measured with thermal–optical carbon analysis by factors of 1.3 and 3.9 for dry and moist spruce combustion in a masonry heater, respectively, and by factors of 2.0 and 3.0 for beech and moist spruce combustion in a chimney stove, respectively. This agrees well with the previously observed SP-HR-ToF-AMS-based OA enhancement factors (1.6–5.3) for RWC (Bertrand et al., 2017; Bruns et al., ~~2015~~2015b; Grieshop et al., 2009; Heringa et al., 2011; Tiitta et al., 2016) and with the thermal-optical analysis-based organic carbon enhancements previously measured for the same chimney stove (1.3–1.4 after 1.7–2.5 eqv.d) (Miersch et al., 2019). The organic carbon concentrations after the PEAR OFR correlated well with the OA measured with SP-HR-ToF-AMS (R^2 = 0.85, Fig. ~~S14~~S15). Aging led to a linear increase in the SP-HR-ToF-AMS-derived ratio of organic matter to organic carbon (OM:OC, Fig. ~~S16~~S17), which rose from the initial average ratio of 1.8–2.2 to 2.7–3.0 during extended aging. Similarly, the OS_C of the OA increased as a function of the photochemical age throughout the tested exposure ranges (Fig. ~~S16~~S17), indicating the existence of continuing reactions of the particulate phase after the rapid consumption of the majority of the primary gaseous SOA precursors with relatively high OH reaction rates (Fig. ~~S11). In contrast, as~~S12). As expected, the organic carbon mass enhancement did not increase with continuous aging because the major SOA precursors were already consumed by relatively short OH exposures. Continuing photochemical exposure may instead reduce the amount of particulate organic carbon (Kroll et al., 2015), which acts as a source for volatile acidic compounds during photochemical aging (Malecha and Nizkorodov, 2016; Paulot et al., 2011). See Table S7 for experiment-wise average concentrations and oxidation states.

The oxidation states measured after the PEAR OFR without oxidative aging were highest for the chimney stove OA, with average unaged OS_Cs of 0.22 and 0.41 for beech and spruce combustion, respectively, while dry and moist spruce in the masonry heater had average unaged OS_Cs of -0.18 and 0.15, respectively. This indicates the existence of different combustion conditions in the studied appliances, with the masonry heater having lower emissions of highly oxygenated compounds and a higher share of unsaturated hydrocarbons compared to that of the chimney stove emissions. However, as a result of oxidative aging, OS_C surpassed 1.5 after 5 eqv.d regardless of the type of experiment~~.~~, which exceeds the values typically observed in ambient aerosol (Kroll et al. 2011, Ng et al. 2011). This is~~A higher initial oxidation state in the chimney stove exhaust led to shallower slopes (-0.17 and -0.34) in the van Krevelen diagram than those in the masonry heater exhaust (-0.46 and -0.49, Fig. 8). Previously, the aging of spruce combustion exhaust from a masonry heater in a chamber has produced similar but slightly steeper van Krevelen slopes of -0.64 – -0.67 (Tiitta et al., 2016). The steepness may be affected by the lower aging and consequent lower final OS_C (maximum of +0.14) as the O:C ratio has been noted to level off at higher oxidation states (Ng et al., 2011). Slopes are also positively affected by fragmentation which may be enhanced in the PEAR because of the more intensive UV radiation than in smog chambers or in ambient conditions. The OS_C of highly aged exhaust exceeds that observed in ambient aerosol (Kroll et al. 2011, Ng et al. 2011),~~ likely because highly aged aerosol in ambient air is mixed continuously with fresh and less oxidised sources. However, the chemical evolution of OA in the PEAR ~~did follow~~OFR followed a similar trend to that observed for typical ambient semi-volatile oxygenated aerosol~~ which had~~, with a van Krevelen slope of -0.5~~ pointing to e.g.~~, which can be

interpreted as a result of simultaneous fragmentation and acid-group addition (Ng et al., 2011). Furthermore, the changes in OS_Cs were similar to those previously observed for ambient aerosol aged extensively in ~~an~~a potential aerosol mass (PAM; Kang et al., 2007) OFR (OS_C up to 2, Ortega et al., 2016~~), and the van Krevelen slopes agreed well with those previously measured from single precursors~~). The OS_Cs of RWC exhaust aged in ~~an oxidation reactor, such as -0.48 for toluene or -0.46 for xylene (Lambe et al., 2011~~a PAM OFR have, however, been notably lower than observed here (Fig. 6; Bruns et al., 2015a; Pieber et al., 2018).

A higher initial oxidation state in the chimney stove exhaust led to shallower slopes (-0.17 and -0.34) in the van Krevelen diagram than those in the masonry heater exhaust (-0.46 and -0.49, Fig. 6). The slope for the beech combustion aerosol was higher than for spruce, which may result from differences in fuel composition as has been observed also previously for biomass burning OA (Ortega et al. 2013). Previously, the aging of spruce combustion exhaust from a masonry heater in a chamber has produced similar but slightly steeper van Krevelen slopes of -0.64 – -0.67 (Tiitta et al., 2016). The steepness may be affected by the shorter aging (< 1 eqv.d) and consequent lower final OS_C (maximum of +0.14) in the chamber, as the O:C ratio has been noted to level off at higher oxidation states (Ng et al., 2011). Slopes are also positively affected by fragmentation which may be enhanced in the PEAR OFR because of the more intensive UV radiation than in smog chambers or in ambient conditions. The van Krevelen slopes agreed well with those previously measured from single precursors aged in the PAM OFR, such as -0.48 for toluene or -0.46 for xylene (Lambe et al., 2011). Similar slopes have been observed also for aging of OA from pellet combustion (-0.47 – -0.44; Czech et al. 2017) or open biomass combustion (-0.5; Ortega et al. 2013) with a PAM OFR.

The evolution of particulate organic aerosol was assessed also by the IDTD-GC-ToFMS analysis of filter samples. When comparing the concentrations in the exhaust after the PEAR OFR, the concentrations of compounds with high oxidation states and low number of carbons (n_C) increased during photochemical aging (upper-right corner of Fig. ~~10~~7). The locations of the measured organic compounds in the OS_C:n_C space are shown in Figure ~~S19~~S20, and their dilution-corrected concentrations downstream the PEAR OFR in Table S12. In the OS_C:n_C space, the compounds which exhibited a major increase during photochemical aging were located in or above the location of the low-volatility oxidised organic aerosol (LV-OOA) classified by Kroll et al. (2011). These compounds are products of the multistep oxidation process including both fragmentation and oxidative reactions.

OA formation is tied to the availability of organic precursors, and thus the formation of SOA was highest at the ignition phase of each batch (Fig. ~~S15~~S16). In the masonry heater, the aged particulate OA mass increased considerably with the introduction of moist logs, simultaneously with the increase in gaseous organics in the fresh emissions. In contrast, the low organic emission by dry spruce combustion was reflected as a lower SOA formation. Another aspect related to the primary exhaust was the extent of OH exposure in the PEAR OFR, which was directly connected to the sample concentrations, as discussed in Chapter 3.3.~~2; namely~~ Namely, the photochemical aging was lower during periods of high emission, leading to lower oxidation states for the OA emitted during ignition.

3.5.2 PMF analysis of particulate OA composition

PMF analysis applied to the exhaust produced a four-factor solution for the OA covering 98 % of the spectra. The spectra of the factors are shown in Figure ~~S17~~S18. Two of the factors were associated in particular with the primary OA from biomass combustion: pyrolysis-BBOA, formed especially during ignition, and flaming-BBOA, emitted pronouncedly during the flaming phase. The other two factors, semi-volatile oxygenated OA (SV-OOA) and low-volatility oxygenated OA (LV-OOA), represent oxygenated organics with notably higher OS_Cs than those of the primary OA factors (Table

3). Flaming-BBOA comprised 76 % and 55 % of the unaged OA from dry and moist spruce combustion in the masonry heater, respectively, but only 27 % and 23 % in the beech and moist spruce combustion OA from the chimney stove, respectively (Fig. ~~10~~8), indicating a less-oxidising higher-temperature flaming phase in the modern masonry heater. Flaming-BBOA is strongly related to the $C_4H_9^+$ -ion (main peak of m/z 57, R^2 = 0.90, Fig. ~~S18)~~S19), which is used as a tracer for hydrocarbon-like compounds (Aiken et al., 2009). However, in contrast to the typical hydrocarbon-like OA factor characterised by a relatively low OS_C (-1.7 to -1.6, Kroll et al., 2011), the flaming-BBOA contains more oxygen-containing functional groups, and is similar to the primary biomass burning OA factor measured in the RWC exhaust in a chamber (Tiitta et al., 2016; θ = 13.6°, R^2 = 0.95). Pyrolysis-BBOA, on the other hand, consisted of ions typical to the low-temperature pyrolysis products of wood combustion and correlated well with the PACs (R^2 = 0.86, Fig. ~~S18~~S19).

Of the more-oxygenated factors, the LV-OOA was dominated by the CO^+ and CO_2^+ ions and thus represented highly oxidised OA. The LV-OOA spectra corresponded well with the OH-induced SOA factor identified from the RWC exhaust aged in a smog chamber (Tiitta et al., 2016., θ = 8.4°, R^2= 0.98), and was comparable with that of ambient LV-OOA (Aiken et al., 2009) and the LV-OOA spectra of unaged wood combustion exhaust (Kortelainen et al., 2018). LV-OOA was also present in the unaged exhaust of this study, excluding the dry spruce combustion in the masonry heater, which produced the least-oxidised primary exhaust. The SV-OOA, on the other hand, was related to the $C_2H_3O^+$-ion (R^2 = 0.78), which is indicative of carbonyl formation in the particulate OA (Ng et al., 2010). The SV-OOA was also comparable (θ = 11.5 °, R^2 = 0.96) to a factor of SOA generated in a chamber in the previous work (Tiitta et al., 2016~~)~~), where this factor was~~-~~ interpreted as ozonolysis-generated organic OA. Interestingly, SV-OOA was formed only during photochemical aging and increased in line with higher exposures despite semi-volatile compounds being products of the initial stages of OA oxidation. This further demonstrates the long-continuing functionalisation of OA during aging alongside with the fragmentation processes.

3.5.3 Polycyclic aromatic compounds

PACs were overall more prominent in the primary exhaust of dry spruce combustion (3.2 % of total OA, Fig. ~~11~~9) than ~~in~~from combustion of moist spruce (1.7 % or 2.0 %) or beech (1.7 %). As expected, the total PAC concentrations decreased because of aging and contributed less than 0.5 % to OA for all cases after 3 eqv.d of aging. Furthermore, aging transformed the composition of the PACs assessed with the SP-HR-ToF-AMS HR-PAH analysis (P-~~MPIP~~MIP analysis, Chapter S5.2; Herring et al., 2015). While UnSubPAHs formed the most prominent PAC group of all the combustion experiments, aging decreased their share from 60 % in unaged exhaust to 40–50 % after 3 eqv.d of aging. Similarly to the PACs measured with SP-HR-ToF-AMS, aging decreased the UnSubPAHs analysed with IDTD-GC-ToFMS by 83–85 % in the dry spruce combustion in the masonry heater, and by 90–98 % in the other situations. Of the most prominent UnSubPAHs, anthracene and fluoranthene degraded within the first eqv.d (Fig. ~~12~~10). Also benzo[a]pyrene, which is a used as the marker for total ambient PAHs (EC 2004), degraded by a factor of 5 ~~because of~~as a result of photochemical aging (Table S12).

The ~~decrease~~change in ~~total PAC concentration likely diminished~~ the ~~adverse~~PACs also alters the potential health effects of the exhaust~~; however, there was a~~: although the total PAC concentration decayed, the simultaneous formation of oxy- and nitro-PAC derivatives known to be detrimental to health was observed. These substituted PACs have lower vapour pressures compared to those of parent PAHs and thus are more likely to condense on the particles (Shen et al., 2012). The share of oxygenated PACs ~~(OPAHs)~~ to the total HR-PAH concentration measured by SP-HR-ToF-AMS increased from 15–19 % in unaged exhaust to 25–38 % in aged exhaust. The concentrations of both the SP-

HR-ToF-AMS HR-OPAH and IDTD-GC-ToFMS derived OH-PAH also correlated with the SV-OOA PMF factor (Pearson r = 0.70 for OPAH and r = 0.88 for OH-PAH; see Table S11) pointing towards their continuous formation during aging. Of the compounds measured by IDTD-GC-ToFMS, the most notable increase was observed for naphthaldehydic acid, with high concentrations in aged aerosol (up to 100 µg m^{-3}) in aged aerosol.dilution corrected flue gas). Interestingly, its concentration was highest at approximately 1 eqv.d, after which it decreased. Naphthaldehydic acid and other oxygenated PAHsPACs have also been previously found to form during photochemical aging of RWC exhaust (Bruns et al., 20152015b; Miersch et al., 2019); however, we found that the photochemically enhanced naphthaldehydic acid concentration degraded after continuous aging, although remaining considerably higher than those in the unaged emissions.

In addition, the share of nitrogen-substituted PAHsPACs, including both NPAH and APAH, increased from a combined share of 5 % of HR-PAH_{tot} (measured by SP-HR-ToF-AMS) in fresh exhaust to a maximum of 9 % in the aged exhaust. In general, particulate nitrogen-substituted PAHsPACs are formed in the atmosphere through the oxidation of gaseous PACs or via heterogenous reactions from UnSubPAHs and are also simultaneously degraded by photochemical reactions (Keyte et al., 2013). As UnSubPAHs in the present study were largely consumed after 3 eqv.d, the higher photochemical exposure times consequently led to a decrease insituation where the precursors for nitrogen-substituted PAHsPACs are not available and therefore no further formation took place.

3.5.4 Organic acids

Photochemical aging led to a considerable increase in particulate organic acids in exhaust aerosol. analysed with IDTD-GC-ToF-MS. The amount of small multifunctional acids such as malic acid ($C_4H_4O_4$) and tartaric acid ($C_4H_6O_6$) increased by factors up to greater than 200 (Fig. 1210, Table S12). Increases in the amounts of also dicarboxylic acids such as succinic ($C_4H_6O_4$) and glutaric acid ($C_5H_8O_4$) were evident, although to a lesser factor. Compared toThe comparison of IDTD-GC-ToF-MS measurements with the SP-HR-ToF-AMS measurements, revealed that the concentrations of organic acids were connected to both LV- and SV-OOA factors (r > 0.7, Table S11), which also strongly increased during the aging process. This was expected based on the association of SV-OOA with the $C_2H_3O^+$-ion indicating carbonyl formation. In the n_C-OS_C space (Fig. 97), these compounds dominated the upper-right corner with the highest oxidation states and largest enhancement ratios and are close to the LV-OOA region specified for atmospheric OA by Kroll et al. (2011). TheseThe measured organic acids were mostly intermediately volatile products of the continuous fragmentation process and partitioned also to the gaseous phase where they in turn participatedare expected to participate in secondary gas-phase OH reactions. TheirOverall, the concentrations of particulate organic acids were highest at approximately 3 eqv.d, after which they were degraded by further oxidation reactions.

3.5.5 Nitrophenols

An increase in nitrophenols in the particulate phase was evident during photochemical aging, which increased the concentrations of 4-nitrophenol (4-NP) and 4-nitrocatechol (4-NC) by respective factors of 2–30 and 30–3000 compared to non-aged exhaust (Fig. 14).10, Table S12) as measured by IDTD-GC-ToFMS. The highest attained 4-NC concentration corresponded to 2 % of total SP-HR-ToF-AMS-based OA concentration, which is a notable fraction for a single compound in an aging aerosol. These secondary nitrophenols were products of OH + phenolic-compound reactions and may have originated from both the gas-phase and heterogenous reactions (Harrison et al., 2005). However,Also the ozonolysis in the presence of NO_2experiments led to an extensive formation of 4-NP, whereas the amount of 4-NC did

not increase. This discrepancy might be the result of absence of the photochemical production of catechol, which is the precursor for 4-NC formation (Finewax et al., 2018).

Nitrophenol concentrations were highest at relatively low OH exposures (1–2 eqv.d) and decreased with increased aging. Similar trends with OH exposure were seen in the NPAH and APAH concentrations measured with SP-HR-ToF-AMS. Nitrophenols are reactive towards OH and photolysis in both gaseous and particulate phases, and ~~as~~ their amount decreased from both phases after the first equivalent days of aging~~, it can be concluded that they overall diminished from~~. Thus, the ~~exhaust with~~measured nitrophenols decay efficiently under high OH-exposures, and therefore are not ideal biomass combustion markers for long-~~term aging. However~~range transported smoke. On the hand, their concentrations ~~did remain~~still remained higher in the highly aged exhaust than in the fresh exhaust. Furthermore, in the particulate phase, they likely contributed to the formation of organic acids which are formed during the continuous photo-oxidation of the nitrophenols (Hems and Abbatt, 2018).

4 Conclusions

The photochemical aging of dynamically changing OA emitted from RWC was evaluated using the PEAR ~~oxidation flow reactor~~OFR to expose the exhaust to varying photochemical conditions for up to an equivalent of one week in the atmosphere. To evaluate typical Northern and Central European combustion emissions, two different appliances were used with regionally typical logwood fuels. While the primary concentrations of particulate OA were relatively similar for all of the assessed sources, the enhancement of the organic particulate carbon during aging depended on the type of the fuel. In particular, the fuel moisture content affected the SOA production~~ with~~: dry fuel ~~producing~~produced a ~~smaller~~lower organic mass and OA enhancement during aging than moist wood, because ~~the OA enhancement was strongly influenced by the~~ of the significantly lower emission rates of the organic gases~~, which were significantly lower for dry spruce.~~. However, a very low (5 %) logwood moisture content ~~also~~ considerably increased the primary PM_1 emission because of the extensive soot formation. With current logwood combustion appliances, this presents a conflict in ~~emission reduction intended to decrease the different constituents in RWC exhaust with overly dry logwood producing large black carbon emissions and moist fuel increasing oxygenated emissions.~~attempts to decrease emissions since the usually preferred dry logwood produces high BC emissions while high moisture content of the fuel increases the amount of organic emissions, as shown here for spruce logwood. Similar phenomenon has, however, been recently noted also for hardwood fuels (Tissari et al., 2019).

The particulate organic carbon mass in the RWC exhaust increased by a factor of 1.3–3.9 during photochemical aging. Furthermore, photochemical aging transformed the overall composition of the OAs. This was observed as a linear increase in the average carbon oxidation state of particulate OA throughout the investigated photochemical exposure range, while the ratio of organic carbon to total organic mass decreased. Photochemical aging caused multiform changes in the OA also at the molecular level. Notably, small~~,~~ acidic reaction and fragmentation products became increasingly dominant in both particulate and gaseous phases with higher aging. The concentrations of particulate nitrophenols were at their highest level after 1 eqv.d, after which they began to ~~decaying~~decay but remained higher than that in the primary exhaust. Similarly, nitrogen-containing aromatics were unobservable in the gaseous phase at longer exposures, although they have been observed to increase during exposures less than 1 eqv.d (Hartikainen et al., 2018). Aging also enhanced the share of oxygen- and nitrogen-substituted polycyclic aromatic compounds in the PAC emissions. Of the oxygenated PACs, naphthaldehydic acid in particular increased considerably with concentrations peaking at approximately 1 eqv.d. However, PACs in total degraded almost completely after 3 eqv.d of aging.

~~Based on this work,~~ In general, several different oxidation mechanisms of organic aerosol are likely occurring simultaneously both in the atmosphere and in the OFR experiments of this study. However, based on the observed OA chemical compositions under a range of different OH-exposures, different major transformation ~~pathways~~mechanisms for RWC exhaust under photochemical conditions can be roughly outlined~~: the initial pathways consisting of functionalisation and~~. First, the results demonstrate that short OH-exposures (~1 eqv.d) are sufficient to functionalize the majority of gaseous SOA precursors of RWC exhaust and lead to their condensation ~~from gaseous precursors are followed by more~~into particulate~~-~~ phase ~~driven chemistry consisting of~~. This mechanism dominates the overall OA transformation until the SOA precursors have been depleted. After this stage, the continuing OH-exposure leads to further oxidation of particulate organic aerosol, which is likely explained by heterogeneous ~~oxidation and fragmentation.~~ reactions between gas-phase oxidants and particles. However, it is also possible that particulate phase oxidation occurs via evaporation and homogeneous gas-phase oxidation followed by recondensation.

While several recent studies (Bertrand et al., 2017; Bruns et al., ~~2015~~2015b; Bruns et al., 2017; Grieshop et al., 2009; Hartikainen et al., 2018; Heringa et al., 2011; Pieber et al., 2018; Tiitta et al., 2016) have assessed the behaviour of RWC emissions in a relatively short timescale of less than ~~1.5~~2 eqv.d, ~~the results of~~ this study ~~emphasise~~highlights the importance of ~~investigating longer photochemical exposures. This is particularly relevant considering~~also higher exposure levels towards chemical transformation of OA. Due to the potentially long atmospheric lifetimes of OA ~~and its importance~~, long-term aging is also important to consider in large-scale atmospheric models, which typically estimate SOA formation and characteristics based on short-term ~~chamber experiments. Atmospheric OA is a mixture of emissions from various sources having diverse exposure levels from fresh emissions to~~ aging experiments. The consideration of only the first stage of gas-phase functionalization and condensation may lead to underestimated oxygenation of the long-transported ~~highly oxidised OAs. The~~OA, while specific compound groups, such as nitrophenols or substituted-PACs, can be overestimated. In general, the potential health and climate effects of aerosols are to a large extent determined by their composition, which depends on their sources and the levels of atmospheric aging. Thus, the characterisation of aerosol emissions from different sources and their atmospheric transformation at different exposure levels ~~is~~would be crucial ~~when assessing~~for assessment of the overall environmental effects of ambient air pollution.

Data availability

The data is available on request from the corresponding author.

Author contributions

AH, OS, PYP, MI, and HL designed the study. Measurements were performed by AH, PT, MI, PYP, MK, HL, HS, JT, and OS. AH, HC, MI, and OS made the assessments of the PEAR conditions. AH performed analyses of FTIR, SMPS, and PTR-ToF-MS data, PT and LH performed the AMS data analyses, JO performed IDTD-GC-ToFMS analyses, and HK performed the thermo-optical analyses. OS, JT, RZ, and JJ supervised and acquired funding to the study. Paper was written by AH with contribution from all ~~the~~ co-authors.

Competing interests

The authors declare that they have no conflict of interest.

Acknowledgements

We thank Donna Sueper from Aerodyne Research, Inc, for her support in the SP-HR-ToF-AMS HR-PAH analysis. Financial support by the Academy of Finland (ASTRO-project (Grant 304459) and NABCEA-project (Grant 296645)), Doctoral School of University of Eastern Finland, German Research Foundation grant ZI 764/14-1, and the Helmholtz virtual Institute HICE (www.hice-vi.eu; InhaleHICE) and the aeroHEALTH Helmholtz International Lab. (www.aerohealth.eu) is gratefully acknowledged.

References

Aiken, A. C., Salcedo, D., Cubison, M. J., Huffman, J. A., DeCarlo, P. F., Ulbrich, I. M., Docherty, K. S., Sueper, D., Kimmel, J. R., Worsnop, D. R., Trimborn, A., Northway, M., Stone, E. A., Schauer, J. J., Volkamer, R. M., Fortner, E., de Foy, B., Wang, J., Laskin, A., Shutthanandan, V., Zheng, J., Zhang, R., Gaffney, J., Marley, N. A., Paredes-Miranda, G., Arnott, W. P., Molina, L. T., Sosa, G. and Jimenez, J. L.: Mexico City aerosol analysis during MILAGRO using high resolution aerosol mass spectrometry at the urban supersite (T0)–Part 1: Fine particle composition and organic source apportionment, Atmos. Chem. Phys., 9, 6633-6653, doi:10.5194/acp-9-6633-2009, 2009.

Atkinson, R., Baulch, D. L., Cox, R. A., Crowley, J. N., Hampson Jr, R. F., Kerr, J. A., Rossi, M. J. and Troe, J.: Summary of evaluated kinetic and photochemical data for atmospheric chemistry, IUPAC Subcommittee on Gas Kinetic Data Evaluation for Atmospheric Chemistry Web Version December 2001, 1-56, 2001.

Avagyan, R., Nyström, R., Lindgren, R., Boman, C. and Westerholm, R.: Particulate hydroxy-PAH emissions from a residential wood log stove using different fuels and burning conditions, Atmos. Environ., 140, 1-9, doi:10.1016/j.atmosenv.2016.05.041, 2016.

Bahreini, R., Ervens, B., Middlebrook, A. M., Warneke, C., de Gouw, J. A., DeCarlo, P. F., Jimenez, J. L., Brock, C. A., Neuman, J. A., Ryerson, T. B., Stark, H., Atlas, E., Brioude, J., Fried, A., Holloway, J. S., Peischl, J., Richter, D., Walega, J., Weibring, P., Wollny, A. G., and Fehsenfeld, F. C. Organic Aerosol Formation in Urban and Industrial Plumes near Houston and Dallas, Texas. J. Geophys. Res. Atmos, 114, doi:10.1029/2008JD011493, 2009

Barmet, P., Dommen, J., DeCarlo, P. F., Tritscher, T., Praplan, A. P., Platt, S. M., Prévôt, A. S. H., Donahue, N. M. and Baltensperger, U.: OH clock determination by proton transfer reaction mass spectrometry at an environmental chamber, Atmos. Meas. Tech., 5, 647, doi:10.5194/amt-5-647-2012, 2012.

Bertrand, A., Stefenelli, G., Bruns, E. A., Pieber, S. M., Temime-Roussel, B., Slowik, J. G., Prévôt, A. S. H. Wortham, H., El Haddad, I. and Marchand, N.: Primary emissions and secondary aerosol production potential from woodstoves for residential heating: Influence of the stove technology and combustion efficiency, Atmos. Environ., 169, 65-79, doi:10.1016/j.atmosenv.2017.09.005, 2017.

Bertrand, A., Stefenelli, G., Jen, C. N., Pieber, S. M., Bruns, E. A., Ni, H., Temime-Roussel, B., Slowik, J. G., Goldstein, A. H., El Haddad, I., Baltensperger, U., Prévôt, A. S. H., Wortham, H. and Marchand, N.: Evolution of the chemical fingerprint of biomass burning organic aerosol during aging, Atmos. Chem. Phys., 18, 7607-7624, doi:10.5194/acp-18-7607-2018, 2018.

Bhattu, D., Zotter, P., Zhou, J., Stefenelli, G., Klein, F., Bertrand, A., Temime-Roussel, B., Marchand, N., Slowik, J. G., Baltensperger, U., Prévôt, A. S. H., Nussbaumer, T., El Haddad, I. and Dommen, J.: Effect of stove technology and

combustion conditions on gas and particulate emissions from residential biomass combustion, Environ. Sci. Technol., 53, 2209-2219, doi:10.1021/acs.est.8b05020, 2019.

Bølling, A. K., Pagels, J., Yttri, K. E., Barregard, L., Sallsten, G., Schwarze, P. E. and Boman, C.: Health effects of residential wood smoke particles: the importance of combustion conditions and physicochemical particle properties, Part. Fibre Toxicol., 6, 29, doi:10.1186/1743-8977-6-29, 2009.

Bruns, E. A., El Haddad, I., Keller, A., Klein, F., Kumar, N. K., Pieber, S. M., Corbin, J. C., Slowik, J. G., Brune, W. H. and Baltensperger, U. and Prévôt, A. S. H.: Inter-comparison of laboratory smog chamber and flow reactor systems on organic aerosol yield and composition, Atmos.Meas.Tech, 8, 2315-2332, doi:10.5194/amt-8-2315-2015, 2015a.

Bruns, E. A., Krapf, M., Orasche, J., Huang, Y., Zimmermann, R., Drinovec, L., Močnik, G., El-Haddad, I., Slowik, J. G., Dommen, J., Baltensperger, U. and Prévôt, A. S. H.: Characterization of primary and secondary wood combustion products generated under different burner loads, Atmos. Chem. Phys., 15, 2825-2841, doi:10.5194/acp-15-2825-2015, 2015b.

Bruns, E. A., Slowik, J. G., El Haddad, I., Kilic, D., Klein, F., Dommen, J., Temime-Roussel, B., Marchand, N., Baltensperger, U. and Prévôt, A S H: Characterization of gas-phase organics using proton transfer reaction time-of-flight mass spectrometry: fresh and aged residential wood combustion emissions, Atmos. Chem. Phys., 17, 705-720, doi:10.5194/acp-17-705-2017, 2017.

Bruns, E. A., El Haddad, I., Slowik, J. G., Kilic, D., Klein, F., Baltensperger, U. and Prévôt, A. S.: Identification of significant precursor gases of secondary organic aerosols from residential wood combustion, Sci. Rep., 6, doi:10.1038/srep27881, 2016.

Canagaratna, M. R., Jimenez, J. L., Kroll, J. H., Chen, Q., Kessler, S. H., Massoli, P., Hildebrandt Ruiz, L., Fortner, E., Williams, L. R., Wilson, K. R., Surratt, J. D., Donahue, N. M., Jayne, J. T. and Worsnop, D. R.: Elemental ratio measurements of organic compounds using aerosol mass spectrometry: characterization, improved calibration, and implications, Atmospheric Chemistry and Physics, 15, 253-272, doi:10.5194/acp-15-253-2015, 2015.

Cappellin, L., Karl, T., Probst, M., Ismailova, O., Winkler, P. M., Soukoulis, C., Aprea, E., Märk, T. D., Gasperi, F. and Biasioli, F.: On quantitative determination of volatile organic compound concentrations using proton transfer reaction time-of-flight mass spectrometry, Environ. Sci. Technol., 46, 2283-2290, doi:10.1021/es203985t, 2012.

Carter, W. P.: Development of ozone reactivity scales for volatile organic compounds, Air & waste, 44, 881-899, 1994.

Czech, H., Miersch, T., Orasche, J., Abbaszade, G., Sippula, O., Tissari, J., Michalke, B., Schnelle-Kreis, J., Streibel, T., Jokiniemi, J. and Zimmermann, R.: Chemical composition and speciation of particulate organic matter from modern residential small-scale wood combustion appliances, Sci. Total Environ., 612, 636-648, doi:10.1016/j.scitotenv.2017.08.263, 2018.

Czech, H., Pieber, S. M., Tiitta, P., Sippula, O., Kortelainen, M., Lamberg, H., Grigonyte, J., Streibel, T., Prévôt, A. S., Jokiniemi, J. and Zimmermann, R.: Time-resolved analysis of primary volatile emissions and secondary aerosol formation potential from a small-scale pellet boiler, Atmos. Environ., 158, 236-245, doi: 10.1016/j.atmosenv.2017.03.040, 2017.

Czech, H., Sippula, O., Kortelainen, M., Tissari, J., Radischat, C., Passig, J., Streibel, T., Jokiniemi, J. and Zimmermann, R.: On-line analysis of organic emissions from residential wood combustion with single-photon ionisation time-of-flight mass spectrometry (SPI-TOFMS), Fuel, 177, 334-342, doi:10.1016/j.fuel.2016.03.036, 2016.

Denier Van Der Gon, H. A. C. , Bergström, R., Fountoukis, C., Johansson, C., Pandis, S. N., Simpson, D. and Visschedijk, A. J.: Particulate emissions from residential wood combustion in Europe–revised estimates and an evaluation, Atmos. Chem. Phys., 15, 6503-6519, doi:10.5194/acp-15-6503-2015, 2015.

Donahue, N. M., Robinson, A. L., Trump, E. R., Riipinen, I. and Kroll, J. H.: Volatility and aging of atmospheric organic aerosol, in: Atmospheric and Aerosol Chemistry, Springer, 97-143, doi: 10.1007/128_2012_355, 2012.

EC (European Council): Directive on relating to arsenic, cadmium, mercury, nickel and polycyclic aromatic hydrocarbons in ambient air, 2004/107/EC, 2004.

Elsasser, M., Busch, C., Orasche, J., Schön, C., Hartmann, H., Schnelle-Kreis, J. and Zimmermann, R.: Dynamic changes of the aerosol composition and concentration during different burning phases of wood combustion, Energy Fuels, 27, 4959-4968, doi:10.1021/ef400684f, 2013.

Finewax, Z., de Gouw, J. A. and Ziemann, P. J.: Identification and Quantification of 4-Nitrocatechol Formed from OH and NO3 Radical-Initiated Reactions of Catechol in Air in the Presence of NOx: Implications for Secondary Organic Aerosol Formation from Biomass Burning, Environ. Sci. Technol., 52, 1981-1989, doi:10.1021/acs.est.7b05864, 2018.

Grieshop, A. P., Logue, J. M., Donahue, N. M. and Robinson, A. L.: Laboratory investigation of photochemical oxidation of organic aerosol from wood fires 1: measurement and simulation of organic aerosol evolution, Atmos. Chem. Phys., 9, 1263-1277, doi:10.5194/acp-9-1263-2009, 2009.

Harrison, M. A., Barra, S., Borghesi, D., Vione, D., Arsene, C. and Olariu, R. I.: Nitrated phenols in the atmosphere: a review, Atmos. Environ., 39, 231-248, doi: 10.1016/j.atmosenv.2004.09.044, 2005.

Hartikainen, A., Yli-Pirilä, P., Tiitta, P., Leskinen, A., Kortelainen, M., Orasche, J., Schnelle-Kreis, J., Lehtinen, K. E., Zimmermann, R., Jokiniemi, J. and Sippula O.: Volatile organic compounds from logwood combustion: emissions and transformation under dark and photochemical aging conditions in a smog chamber, Environ. Sci. Technol., 52, 4979-4988, doi:10.1021/acs.est.7b06269, 2018.

Hatch, L. E., Yokelson, R. J., Stockwell, C. E., Veres, P. R., Simpson, I. J., Blake, D. R., Orlando, J. J. and Barsanti, K. C.: Multi-instrument comparison and compilation of non-methane organic gas emissions from biomass burning and implications for smoke-derived secondary organic aerosol precursors, Atmos. Chem. Phys., 17, 1471-1489, doi:10.5194/acp-17-1471-2017, 2017.

Heald, C. L., Kroll, J. H., Jimenez, J. L., Docherty, K. S., DeCarlo, P. F., Aiken, A. C., Chen, Q., Martin, S. T., Farmer, D. K. and Artaxo, P.: A simplified description of the evolution of organic aerosol composition in the atmosphere, Geophys. Res. Lett., 37, doi:10.1029/2010GL042737, 2010.

Hems, R. F. and Abbatt, J. P.: Aqueous phase photo-oxidation of brown carbon nitrophenols: reaction kinetics, mechanism, and evolution of light absorption, ACS Earth Space Chem., 2, 225-234, doi:10.1021/acsearthspacechem.7b00123, 2018.

Hennigan, C. J., Miracolo, M. A., Engelhart, G. J., May, A. A., Presto, A. A., Lee, T., Sullivan, A. P., McMeeking, G. R., Coe, H., Wold, C. E., Hao, W.-M., Gilman, J. B., Kuster, W. C., de Gouw, J., Schichtel, B. A., Collett Jr., J. L., Kreidenweis, S. M. and Robinson, A. L.: Chemical and physical transformations of organic aerosol from the photo-oxidation of open biomass burning emissions in an environmental chamber, Atmos. Chem. Phys., 11, 7669-7686, doi:10.5194/acp-11-7669-2011, 2011.

Heringa, M. F., DeCarlo, P. F., Chirico, R., Tritscher, T., Dommen, J., Weingartner, E., Richter, R., Wehrle, G., Prévôt, A. and Baltensperger, U.: Investigations of primary and secondary particulate matter of different wood combustion appliances with a high-resolution time-of-flight aerosol mass spectrometer, Atmos. Chem. Phys., 11, 5945-5957, doi:10.5194/acp-11-5945-2011, 2011.

Herring, C. L., Faiola, C. L., Massoli, P., Sueper, D., Erickson, M. H., McDonald, J. D., Simpson, C. D., Yost, M. G., Jobson, B. T. and VanReken, T. M.: New methodology for quantifying polycyclic aromatic hydrocarbons (PAHs) using high-resolution aerosol mass spectrometry, Aerosol Sci. Tech., 49, 1131-1148, doi:10.1080/02786826.2015.1101050, 2015.

Hodzic, A., Madronich, S., Kasibhatla, P. S., Tyndall, G., Aumont, B., Jimenez, J. L., Lee-Taylor, J. and Orlando, J.: Organic photolysis reactions in tropospheric aerosols: effect on secondary organic aerosol formation and lifetime, Atmos. Chem. Phys., 15, 9253-9269, doi:10.5194/acp-15-9253-20152015.

Hodzic, A., Kasibhatla, P. S., Jo, D. S., Cappa, C. D., Jimenez, J. L., Madronich, S. and Park, R. J.: Rethinking the global secondary organic aerosol (SOA) budget: stronger production, faster removal, shorter lifetime, Atmos. Chem. Phys, 16, 7917-7941, doi:10.5194/acp-16-7917-2016, 2016.

Ihalainen, M., Tiitta, P., Czech, H., Yli-Pirilä, P., Hartikainen, A., Kortelainen, M., Tissari, J., Stengel, B., Sklorz, M., Suhonen, H., Lamberg, H., Leskinen, A., Kiendler-Scharr, A., Harndorf, H., Zimmermann, R., Jokiniemi, J. and Sippula, O.: A novel high-volume Photochemical Emission Aging flow tube Reactor (PEAR), Aerosol Sci. Tech., 53, 276-294, doi:10.1080/02786826.2018.1559918, 2019.

Jayne, J. T., Leard, D. C., Zhang, X., Davidovits, P., Smith, K. A., Kolb, C. E. and Worsnop, D. R.: Development of an aerosol mass spectrometer for size and composition analysis of submicron particles, Aerosol. Sci. Technol., 33, 49-70, doi:10.1080/027868200410840, 2000.

Kanashova, T., Sippula, O., Oeder, S., Streibel, T., Passig, J., Czech, H., Kaoma, T., Sapcariu, S. C., Dilger, M., Paur, H., Schlager, C., Mülhopt, S., Weiss, C., Schmidt-Weber, C., Traidl-Hoffmann, C., Michalke, B., Krebs, T., Karg, E., Jakobi, G., Scholtes, S., Schnelle-Kreis, J., Sklorz, M., Orasche, J., Müller, L., Reda, A., Rüger, C., Neumann, A., Abbaszade, G., Radischat, C., Hiller, K., Grigonyte, J., Kortelainen, M., Kuuspalo, K., Lamberg, H., Leskinen, J., Nuutinen, I., Torvela, T., Tissari, J., Jalava, P., Kasurinen, S., Uski, O., Hirvonen, M.-R., Buters, J., Dittmar, G., Jokiniemi, J. K. and Zimmermann, R.: Emissions from a modern log wood masonry heater and wood pellet boiler: Composition and biological impact on air-liquid interface exposed human lung cancer cells, Journal of Molecular and Clinical Medicine, 1, 23-35, doi:10.31083/j.jmcm.2018.01.004, 2018.

Kang, E., Root, M. J., Toohey, D. W. and Brune, W. H.: Introducing the concept of potential aerosol mass (PAM), Atmos. Chem. Phys., 7, 5727-5744, doi:10.5194/acp-7-5727-2007, 2007.

Kasurinen, S., Happo, M. S., Rönkkö, T. J., Orasche, J., Jokiniemi, J., Kortelainen, M., Tissari, J., Zimmermann, R., Hirvonen, M. and Jalava, P. I.: Differences between co-cultures and monocultures in testing the toxicity of particulate matter derived from log wood and pellet combustion, PloS one, 13(2): e0192453, doi:10.1371/journal.pone.0192453, 2018.

Keyte, I. J., Harrison, R. M. and Lammel, G.: Chemical reactivity and long-range transport potential of polycyclic aromatic hydrocarbons–a review, Chem. Soc. Rev., 42, 9333-9391, doi:10.1039/c3cs60147a, 2013.

Kim, K., Jahan, S. A., Kabir, E. and Brown, R. J.: A review of airborne polycyclic aromatic hydrocarbons (PAHs) and their human health effects, Environ. Int., 60, 71-80, doi:10.1016/j.envint.2013.07.019, 2013.

Klimont, Z., Kupiainen, K., Heyes, C., Purohit, P., Cofala, J., Rafaj, P., Borken-Kleefeld, J. and Schöpp, W.: Global anthropogenic emissions of particulate matter including black carbon, Atmos. Chem. Phys., 17, 8681-8723, doi:10.5194/acp-17-8681-2017, 2017.

Kortelainen, M., Jokiniemi, J., Tiitta, P., Tissari, J., Lamberg, H., Leskinen, J., Rodriguez, J. G., Koponen, H., Antikainen, S., Nuutinen, I., Zimmermann, R. and Sippula, O..: Time-resolved chemical composition of small-scale batch combustion emissions from various wood species, Fuel, 233, 224-236, doi:10.1016/j.fuel.2018.06.056, 2018.

Kostenidou, E., Lee, B., Engelhart, G. J., Pierce, J. R. and Pandis, S. N.: Mass spectra deconvolution of low, medium, and high volatility biogenic secondary organic aerosol, Environ. Sci. Technol., 43, 4884-4889, doi:10.1021/es803676g, 2009.

Kroll, J. H., Donahue, N. M., Jimenez, J. L., Kessler, S. H., Canagaratna, M. R., Wilson, K. R., Altieri, K. E., Mazzoleni, L. R., Wozniak, A. S., Bluhm, H., Mysak, E. R., Smith, J. D., Kolb, C. E. and Worsnop, D. R.: Carbon oxidation state as a metric for describing the chemistry of atmospheric organic aerosol, Nat. Chem., 3, 133, doi:10.1038/nchem.948, 2011.

Kroll, J. H., Lim, C. Y., Kessler, S. H. and Wilson, K. R.: Heterogeneous oxidation of atmospheric organic aerosol: kinetics of changes to the amount and oxidation state of particle-phase organic carbon, J. Phys. Chem. A, 119, 10767-10783, doi:10.1021/acs.jpca.5b06946, 2015.

Lambe, A. T., Onasch, T. B., Massoli, P., Croasdale, D. R., Wright, J. P., Ahern, A. T., Williams, L. R., Worsnop, D. R., Brune, W. H. and Davidovits, P.: Laboratory studies of the chemical composition and cloud condensation nuclei (CCN) activity of secondary organic aerosol (SOA) and oxidized primary organic aerosol (OPOA), Atmos. Chem. Phys., 11, 8913-8928, doi: 10.5194/acp-11-8913-2011, 2011.

Lanz, V. A., Alfarra, M. R., Baltensperger, U., Buchmann, B., Hueglin, C. and Prévôt, A.: Source apportionment of submicron organic aerosols at an urban site by factor analytical modelling of aerosol mass spectra, Atmos. Chem. Phys., 7, 1503-1522, doi:10.5194/acp-7-1503-2007, 2007.

Lehtinen, K. E., Korhonen, H., Maso, M. D. and Kulmala, M.: On the concept of condensation sink diameter, Boreal Environ. Res., 8, 405-412, 2003.

Leskinen, J., Tissari, J., Uski, O., Virén, A., Torvela, T., Kaivosoja, T., Lamberg, H., Nuutinen, I., Kettunen, T. and Joutsensaari, J.: Fine particle emissions in three different combustion conditions of a wood chip-fired appliance–Particulate physico-chemical properties and induced cell death, Atmos. Environ., 86, 129-139, doi:10.1016/j.atmosenv.2013.12.012, 2014.

Li, M., Bao, F., Zhang, Y., Song, W., Chen, C. and Zhao, J.: Role of elemental carbon in the photochemical aging of soot, Proceedings of the National Academy of Sciences, 115, 7717-7722, doi:10.1073/pnas.1804481115, 2018.

Li, R., Palm, B. B., Ortega, A. M., Hlywiak, J., Hu, W., Peng, Z., Day, D. A., Knote, C., Brune, W. H., De Gouw, J. A. and Jimenez, J. L.: Modeling the radical chemistry in an oxidation flow reactor: radical formation and recycling, sensitivities, and the OH exposure estimation equation, The Journal of Physical Chemistry A, 119, 4418-4432, doi:10.1021/jp509534k, 2015.

Malecha, K. T. and Nizkorodov, S. A.: Photodegradation of secondary organic aerosol particles as a source of small, oxygenated volatile organic compounds, Environ. Sci. Technol., 50, 9990-9997, doi:10.1021/acs.est.6b02313, 2016.

McDonald, J. D., Zielinska, B., Fujita, E. M., Sagebiel, J. C., Chow, J. C. and Watson, J. G.: Fine Particle and Gaseous Emission Rates from Residential Wood Combustion, Environ. Sci. Technol., 34, 2080-2091, doi:10.1021/es9909632, 2000.

McFiggans, G., Mentel, T. F., Wildt, J., Pullinen, I., Kang, S., Kleist, E., Schmitt, S., Springer, M., Tillmann, R., Wu, C., Zhao, D., Hallquist, M., Faxon, C., Le Breton, M., Hallquist, Å M., Simpson, D., Bergström, R., Jenkin, M. E., Ehn, M., Thornton, J. A., Alfarra, M. R., Bannan, T. J., Percival, C. J., Priestley, M., Topping, D. and Kiendler-Scharr, A.: Secondary organic aerosol reduced by mixture of atmospheric vapours, Nature, 565, 587, doi:10.1038/s41586-018-0871-y, 2019.

Miersch, T., Czech, H., Hartikainen, A., Ihalainen, M., Orasche, J., Abbaszade, G., Tissari, J., Streibel, T., Jokiniemi, J., Sippula, O. and Zimmermann, R.: Impact of photochemical ageing on Polycyclic Aromatic Hydrocarbons (PAH) and oxygenated PAH (Oxy-PAH/OH-PAH) in logwood stove emissions, Sci. Total Environ., 686, 382-392, doi:10.1016/j.scitotenv.2019.05.412, 2019.

Moise, T., Flores, J. M. and Rudich, Y.: Optical properties of secondary organic aerosols and their changes by chemical processes, Chem. Rev., 115, 4400-4439, doi:10.1021/cr5005259, 2015.

Ng, N. L., Canagaratna, M. R., Jimenez, J. L., Chhabra, P. S., Seinfeld, J. H. and Worsnop, D. R.: Changes in organic aerosol composition with aging inferred from aerosol mass spectra, Atmos. Chem. Phys., 11, 6465-6474, doi:10.5194/acp-11-6465-2011, 2011.

Ng, N. L., Canagaratna, M. R., Zhang, Q., Jimenez, J. L., Tian, J., Ulbrich, I. M., Kroll, J. H., Docherty, K. S., Chhabra, P. S., Bahreini, R., Murphy, S. M., Seinfeld, J. H., Hildebrandt, L., Donahue, N. M., DeCarlo, P. F., Lanz, V. A., Prévôt, A. S. H., Dinar, E., Rudich, Y. and Worsnop, D. R.: Organic aerosol components observed in Northern Hemispheric datasets from Aerosol Mass Spectrometry, Atmos. Chem. Phys., 10, 4625-4641, doi:10.5194/acp-10-4625-2010, 2010.

Nuutinen, K., Jokiniemi, J., Sippula, O., Lamberg, H., Sutinen, J., Horttanainen, P. and Tissari, J.: Effect of air staging on fine particle, dust and gaseous emissions from masonry heaters, Biomass Bioenergy, 67, 167-178, doi:10.1016/j.biombioe.2014.04.033, 2014.

Onasch, T. B., Trimborn, A., Fortner, E. C., Jayne, J. T., Kok, G. L., Williams, L. R., Davidovits, P. and Worsnop, D. R.: Soot Particle Aerosol Mass Spectrometer: Development, Validation, and Initial Application, Aerosol Sci. Tech., 46, 804-817, doi:10.1080/02786826.2012.663948, 2012.

Orasche, J., Schnelle-Kreis, J., Abbaszade, G. and Zimmermann, R.: In-situ derivatization thermal desorption GC-TOFMS for direct analysis of particle-bound non-polar and polar organic species, Atmos. Chem. Phys., 11, 8977-8993, doi:10.5194/acp-11-8977-2011, 2011.

Orasche, J., Schnelle-Kreis, J., Schön, C., Hartmann, H., Ruppert, H., Arteaga-Salas, J. M. and Zimmermann, R.: Comparison of emissions from wood combustion. Part 2: Impact of combustion conditions on emission factors and characteristics of particle-bound organic species and polycyclic aromatic hydrocarbon (PAH)-related toxicological potential, Energy Fuels, 27, 1482-1491, doi:10.1021/ef301506h, 2013.

Ortega, A. M., Day, D. A., Cubison, M. J., Brune, W. H., Bon, D., de Gouw, J. A., and Jimenez, J. L.: Secondary organic aerosol formation and primary organic aerosol oxidation from biomass-burning smoke in a flow reactor during FLAME-3, Atmos. Chem. Phys., 13, 11551–11571, doi:10.5194/acp-13-11551-2013, 2013.

Ortega, A. M., Hayes, P. L., Peng, Z., Palm, B. B., Hu, W., Day, D. A., Li, R., Cubison, M. J., Brune, W. H., Graus, M., Warneke, C., Gilman, J. B., Kuster, W. C., de Gouw, J., Gutiérrez-Montes, C. and Jimenez, J. L.: Real-time measurements of secondary organic aerosol formation and aging from ambient air in an oxidation flow reactor in the Los Angeles area, Atmos. Chem. Phys., 16, 7411-7433, doi:10.5194/acp-16-7411-2016, 2016.

Palm, B. B., Campuzano-Jost, P., Ortega, A. M., Day, D. A., Kaser, L., Jud, W., Karl, T., Hansel, A., Hunter, J. F., Cross, E. S., Kroll, J. H., Peng, Z., Brune, W. H. and Jimenez, J. L.: In situ secondary organic aerosol formation from ambient pine forest air using an oxidation flow reactor, Atmos. Chem. Phys., 16, 2943-2970, doi:10.5194/acp-16-2943-2016, 2016.

Paulot, F., Wunch, D., Crounse, J. D., Toon, G. C., Millet, D. B., DeCarlo, P. F., Vigouroux, C., Deutscher, N. M., González Abad, G., Notholt, J., Warneke, T., Hannigan, J. W., Warneke, C., de Gouw, J. A., Dunlea, E. J., De Maziére, M., Griffith, D. W. T., Bernath, P., Jimenez, J. L. and Wennberg, P. O.: Importance of secondary sources in the atmospheric budgets of formic and acetic acids, Atmos. Chem. Phys., 11, 1989-2013, doi:10.5194/acp-11-1989-2011, 2011.

Peng, Z., Day, D. A., Ortega, A. M., Palm, B. B., Hu, W., Stark, H., Li, R., Tsigaridis, K., Brune, W. H. and Jimenez, J. L.: Non-OH chemistry in oxidation flow reactors for the study of atmospheric chemistry systematically examined by modeling, Atmos. Chem. Phys., 16, 4283-4305, doi:10.5194/acp-16-4283-2016, 2016.

Peng, Z. and Jimenez, J. L.: Modeling of the chemistry in oxidation flow reactors with high initial NO, Atmos. Chem. Phys., 17, 11991-12010, doi:10.5194/acp-17-11991-2017, 2017.

Peng, Z., Lee-Taylor, J., Orlando, J. J., Tyndall, G. S. and Jimenez, J. L.: Organic peroxy radical chemistry in oxidation flow reactors and environmental chambers and their atmospheric relevance, Atmospheric Chem. Phys., 19(2), 813–834, doi:10.5194/acp-19-813-2019, 2019.

Pieber, S. M., El Haddad, I., Slowik, J. G., Canagaratna, M. R., Jayne, J. T., Platt, S. M., Bozzetti, C., Daellenbach, K. R., Fröhlich, R., Vlachou, A., Klein F., Dommen, J., Miljevic, B., Jiménez J. L., Worsnop D. R., Baltensperger, U. and Prévôt A. S. H.: Inorganic salt interference on CO2 in aerodyne AMS and ACSM organic aerosol composition studies, Environ. Sci. Technol., 50, 10494-10503, doi: DOI:10.1021/acs.est.6b01035, 2016.

Pieber, S. M., Kambolis, A., Ferri, D., Bhattu, D., Bruns, E. A., Elsener, M., Kröcher, O., Prévôt, A. S. and Baltensperger, U.: Mitigation of Secondary Organic Aerosol Formation from Log Wood Burning Emissions by Catalytic Removal of Aromatic Hydrocarbons, Environ. Sci. Technol., 52, 13381-13390, doi: 10.1021/acs.est.8b04124, 2018.

Prinn, R. G., Huang, J., Weiss, R. F., Cunnold, D. M., Fraser, P. J., Simmonds, P. G., McCulloch, A., Harth, C., Reimann, S., Salameh, P., O'Doherty, S., Wang, R. H. J., Porter, L. W., Miller, B. R. and Krummel, P. B.: Evidence for variability of atmospheric hydroxyl radicals over the past quarter century, Geophys. Res. Lett., 32, doi:10.1029/2004GL022228, 2005.

Reda, A. A., Czech, H., Schnelle-Kreis, J., Sippula, O., Orasche, J., Weggler, B., Abbaszade, G., Arteaga-Salas, J., Kortelainen, M., Tissari, J., Jokiniemi, J., Streibel, T. and Zimmermann, R.: Analysis of Gas-Phase Carbonyl Compounds

in Emissions from Modern Wood Combustion Appliances: Influence of Wood Type and Combustion Appliance, Energy Fuels, 29, 3897-3907, doi:10.1021/ef502877c, 2015.

Robinson, A. L., Donahue, N. M., Shrivastava, M. K., Weitkamp, E. A., Sage, A. M., Grieshop, A. P., Lane, T. E., Pierce, J. R. and Pandis, S. N.: Rethinking organic aerosols: semivolatile emissions and photochemical aging, Science, 315, 1259-1262, doi:10.1126/science.1133061, 2007.

Shen, G., Tao, S., Wei, S., Zhang, Y., Wang, R., Wang, B., Li, W., Shen, H., Huang, Y., Chen, Y., Chen, H., Yang, Y., Wang, W., Wang, X., Liu, W. and Simonich, S. L. M.: Emissions of parent, nitro, and oxygenated polycyclic aromatic hydrocarbons from residential wood combustion in rural China, Environ. Sci. Technol., 46, 8123-8130, doi:10.1021/es301146v, 2012.

Simonen, P., Saukko, E., Karjalainen, P., Timonen, H., Bloss, M., Aakko-Saksa, P., Rönkkö, T., Keskinen, J. and Dal Maso, M..: A new oxidation flow reactor for measuring secondary aerosol formation of rapidly changing emission sources, Atmos. Meas. Tech., 10, 1519-1537, doi:10.5194/amt-10-1519-2017, 2017.

Sippula, O., Hokkinen, J., Puustinen, H., Yli-Pirilä, P. and Jokiniemi, J.: Particle emissions from small wood-fired district heating units, Energy Fuels, 23, 2974-2982, doi:10.1021/ef900098v, 2009.

Tiitta, P., Leskinen, A., Hao, L., Yli-Pirilä, P., Kortelainen, M., Grigonyte, J., Tissari, J., Lamberg, H., Hartikainen, A., Kuuspalo, K., Kortelainen, A.-M., Virtanen, A., Lehtinen, K. E. J., Komppula, M., Pieber, S., Prévôt, A. S. H., Onasch, T. B., Worsnop, D. R., Czech, H., Zimmermann, R., Jokiniemi, J. and Sippula, O.: Transformation of logwood combustion emissions in a smog chamber: formation of secondary organic aerosol and changes in the primary organic aerosol upon daytime and nighttime aging, Atmos. Chem. Phys., 16, 13251-13269, doi:10.5194/acp-16-13251-2016, 2016.

Tissari, J., Lyyränen, J., Hytönen, K., Sippula, O., Tapper, U., Frey, A., Saarnio, K., Pennanen, A. S., Hillamo, R., Salonen, R. O., Hirvonen, M. R. and Jokiniemi, J.: Fine particle and gaseous emissions from normal and smouldering wood combustion in a conventional masonry heater, Atmos. Environ., 42, 7862-7873, doi:10.1016/j.atmosenv.2008.07.019, 2008.

Tissari, J., Hytönen, K., Sippula, O. and Jokiniemi, J.: The effects of operating conditions on emissions from masonry heaters and sauna stoves, Biomass Bioenergy, 33, 513-520, doi:10.1016/j.biombioe.2008.08.009, 2009.

Tissari, J., Väätäinen, S., Leskinen, J., Savolahti, M., Lamberg, H., Kortelainen, M., Karvosenoja, N. and Sippula, O.: Fine Particle Emissions from Sauna Stoves: Effects of Combustion Appliance and Fuel, and Implications for the Finnish Emission Inventory, Atmosphere, 10, 775, doi:10.3390/atmos10120775, 2019.

Ulbrich, I. M., Canagaratna, M. R., Zhang, Q., Worsnop, D. R. and Jimenez, J. L.: Interpretation of organic components from Positive Matrix Factorization of aerosol mass spectrometric data, Atmos. Chem. Phys., 9, 2891-2918, doi:10.5194/acp-9-2891-2009, 2009.

United States Environmental Protection Agency (USEPA). Integrated Risk Information System (IRIS); National Center for Environmental Assessment: Washington, DC (http://www.epa.gov/iris, accessed October 21, 2019).

Xu, W., Lambe, A., Silva, P., Hu, W., Onasch, T., Williams, L., Croteau, P., Zhang, X., Renbaum-Wolff, L., Fortner, E., Jimenez, J. L., Jayne, J., Worsnop, D. and Canagaratna, M.: Laboratory evaluation of species-dependent relative

ionization efficiencies in the Aerodyne Aerosol Mass Spectrometer, Aerosol Sci. Tech., 52, 626-641, doi: 10.1080/02786826.2018.1439570, 2018.

Zhang, X., Lin, Y., Surratt, J. D., Zotter, P., Prévôt, A. S. and Weber, R. J.: Light-absorbing soluble organic aerosol in Los Angeles and Atlanta: A contrast in secondary organic aerosol, Geophys. Res. Lett., 38, doi:10.1029/2011GL049385, 2011.

Table 1: Combustion conditions and experimental conditions of each experiment.

	Exp.	hv flux [photons cm^{-2} s^{-1}]	O_3 ~~input~~ [ppm]	Initial age* [eqv. d]	Fuel	OH exp. [# s cm^{-3}]	Age [eqv.d]	MCE	~~VOC~~OGC/NO_x	DR
Masonry heater	1	lamps off	0	no-OH	S-5%			0.979	1.5	64
					S-22%			0.974	4.9	83
	2	8.~~3E~~6E+15	2.3	14.07	S-5%	5.8E+11	6.~~7~~8	0.975	1.2	137
					S-22%	3.5E+11	4.0	0.978	3.1	147
	3	lamps off	2.5	no-OH	S-5%			0.974	1.3	135
					S-22%			0.973	4.0	144
	4	~~1.9E~~2.8E+15	2.2	5.84	S-5%	1.5E+11	1.7	0.974	1.4	130
					S-22%	1.3E+11	1.5	0.966	5.5	152
	5	1.4E+15	1.8	2.35	S-5%	8.1E+10	0.9	0.971	1.3	160
					S-22%	6.3E+10	0.7	0.976	3.7	196
Chimney stove	1	lamps off	0	no-OH	B-17%			0.968	1.6	72
					S-22%			0.966	5.4	80
	2	5.~~4E~~8E+15	4.3	12.90	B-17%	3.1E+11	3.6	0.963	1.8	122
					S-22%	not meas.	~4**	0.965	3.6	148
	3	lamps off	3.1	no-OH	B-17%			0.953	1.9	124
					S-22%			0.961	4.9	143
	4	1.1E+15	3.6	5.10	B-17%	5.4E+10	0.6	0.951	1.7	119
					S-22%	6.1E+10	0.7	0.972	4.2	135
	5	1.1E+16	11	18.76	B-17%	5.0E+11	5.8	0.962	1.5	36
					S-22%	5.0E+11	5.8	0.957	5.6	40

*Age based on the OH-exposure of clean air, prior to sample input.
** Direct OH exposure measurements not available for Chimney stove Exp. 2 S-22%; approximately similar as in Exp. 2 B-17%.

Table 2: Primary PM_1 ~~emissions~~concentrations in dry ~~13% O_2 exhaust~~flue gas. The number concentration and geometric mean mobility diameter (GMD) were derived from a scanning mobility particle sizer and PM1, organic carbon, and elemental carbon from filter samples.

	Number ~~([~~10^7 # cm^{-3}~~)]~~	GMD ~~([~~nm~~)]~~	PM_1 ~~([~~mg m^{-3}~~)]~~	OC ~~([~~mg m^{-3}~~)]~~	EC ~~([~~mg m^{-3}~~)]~~	OC:EC
Masonry heater, spruce 5 % H_2O (S-5%)	3.2 ± 0.6	95.5 ± 24.4	67 ± 16	4.3 ± 1.9	57.1 ± 15.8	0.07 ± 0.02
Masonry heater, spruce 22 % H_2O (S-22%)	4.5 ± 1.6	68.4 ± 22.2	33 ± 16	4.4 ± 4.6	19.1 ± 12	0.31 ± 0.45
Chimney stove, beech 17 % H_2O (B-17%)	4.4 ± 0.4	61.1 ± 7.6	43 ± 11	3.0 ± 1.4	21.9 ± 11.1	0.15 ± 0.04
B-17% : 1st to 2nd batch	4.3 ± 1.9	71.6 ± 5.7	48 ± 4	4.2 ± 0.9	32.0 ± 5.3	0.12 ± 0.01
B-17% : 3rd to 4th batch	5.4 ± 0.9	57.2 ± 5	38 ± 13	1.9 ± 0.6	11.8 ± 3.3	0.18 ± 0.03
Chimney stove, spruce 22 % H_2O (S-22%)	4.5 ± 0.3	52.8 ± 13.3	37 ± 8	4.3 ± 0.7	17.0 ± 2.0	0.25 ± 0.04

Table 3: Properties of the PMF factors.

Factor	O:C	H:C	N:C	OS_C	OM:OC
LV-OOA	1.57	0.97	5.97E-03	2.18	3.19
SV-OOA	0.78	1.41	1.78E-03	0.16	2.17
Flaming-BBOA	0.55	1.52	4.33E-03	-0.42	1.86
Pyrolysis-BBOA	0.49	1.41	2.13E-03	-0.44	1.77

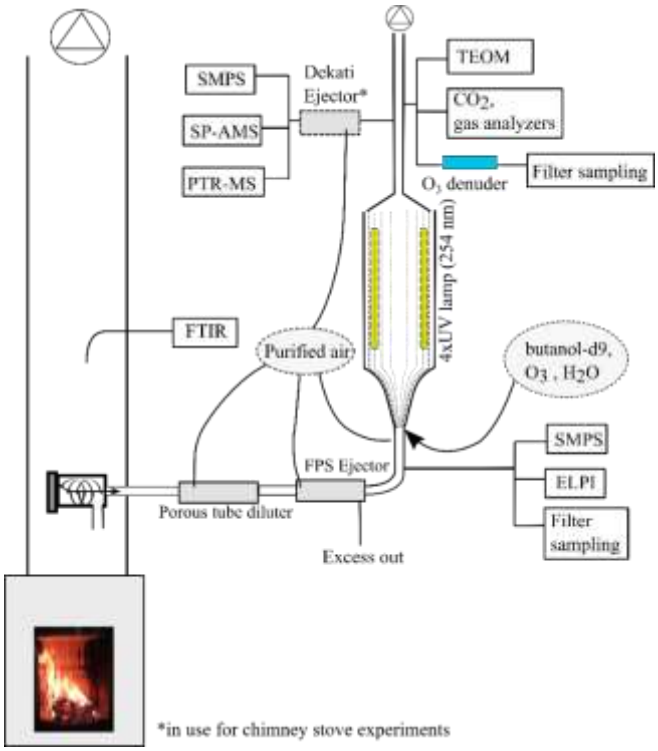

Figure 1: Experimental setup.

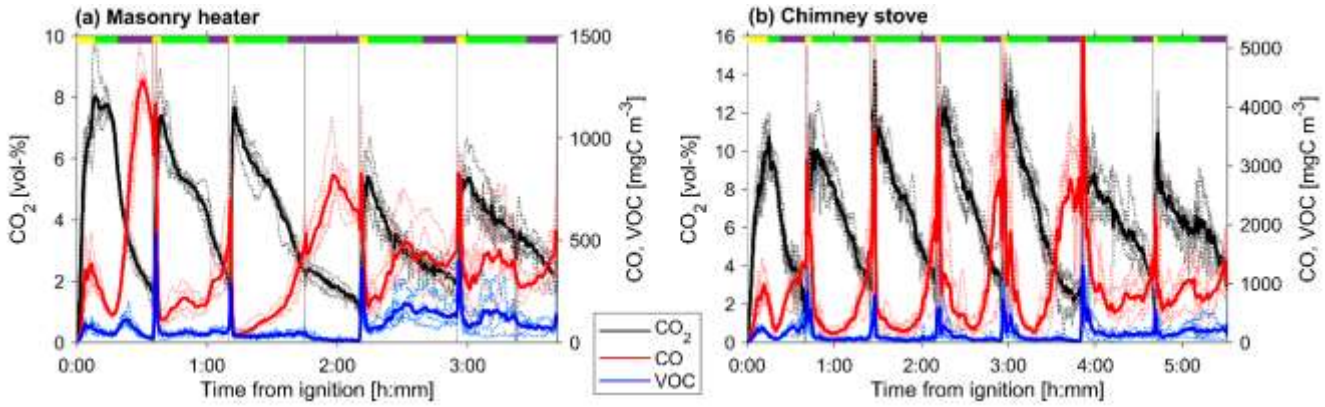

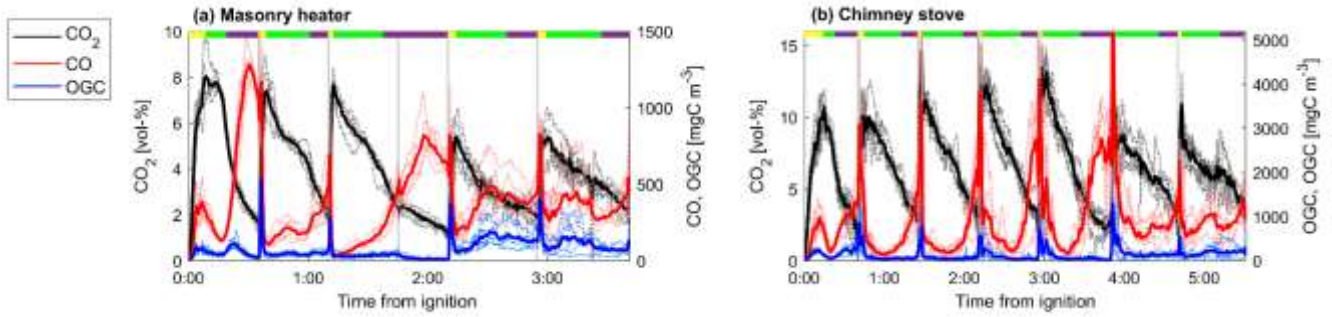

Figure 2: CO_2, and CO, and the ~~VOCs~~OGC in the dry exhaust gas from (a) masonry heater, and (b) chimney stove, measured by FTIR. Averages over all experiments are shown with solid lines, whereas different experiments are shown with dotted lines. Average phase lengths are marked on the top panel with the yellow (ignition), green (flaming), and purple (burnout).

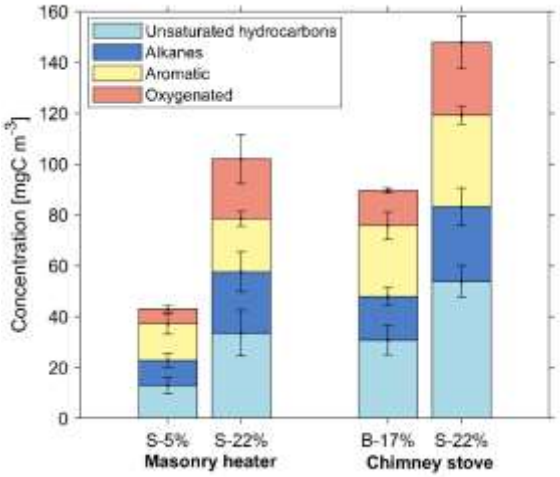

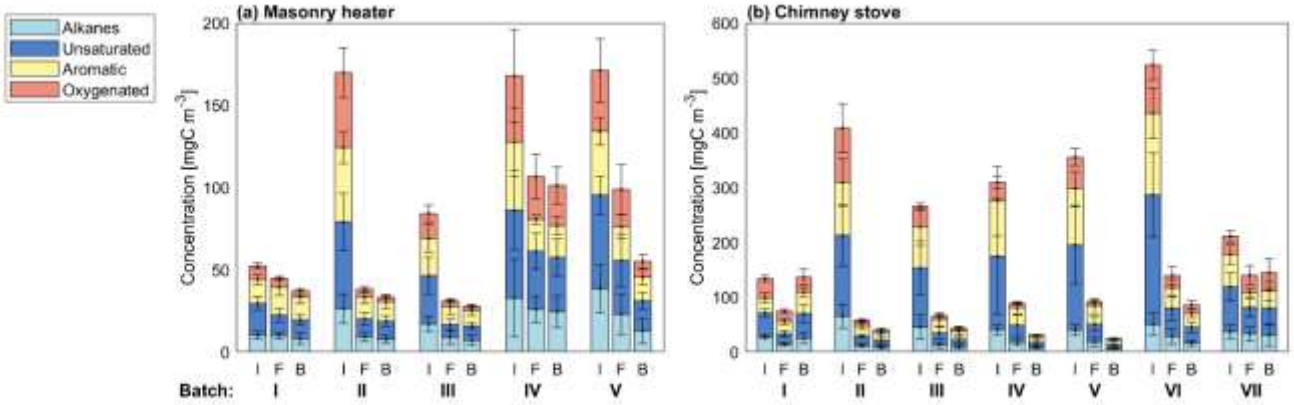

Figure 3: Average concentrations of organic gaseous compounds in the dry primary exhaust at the different combustion phases (I=ignition, F=flaming, B=char burnout phase) for each batch measured by FTIR from the stack. Error bars denote standard deviations between experiments.

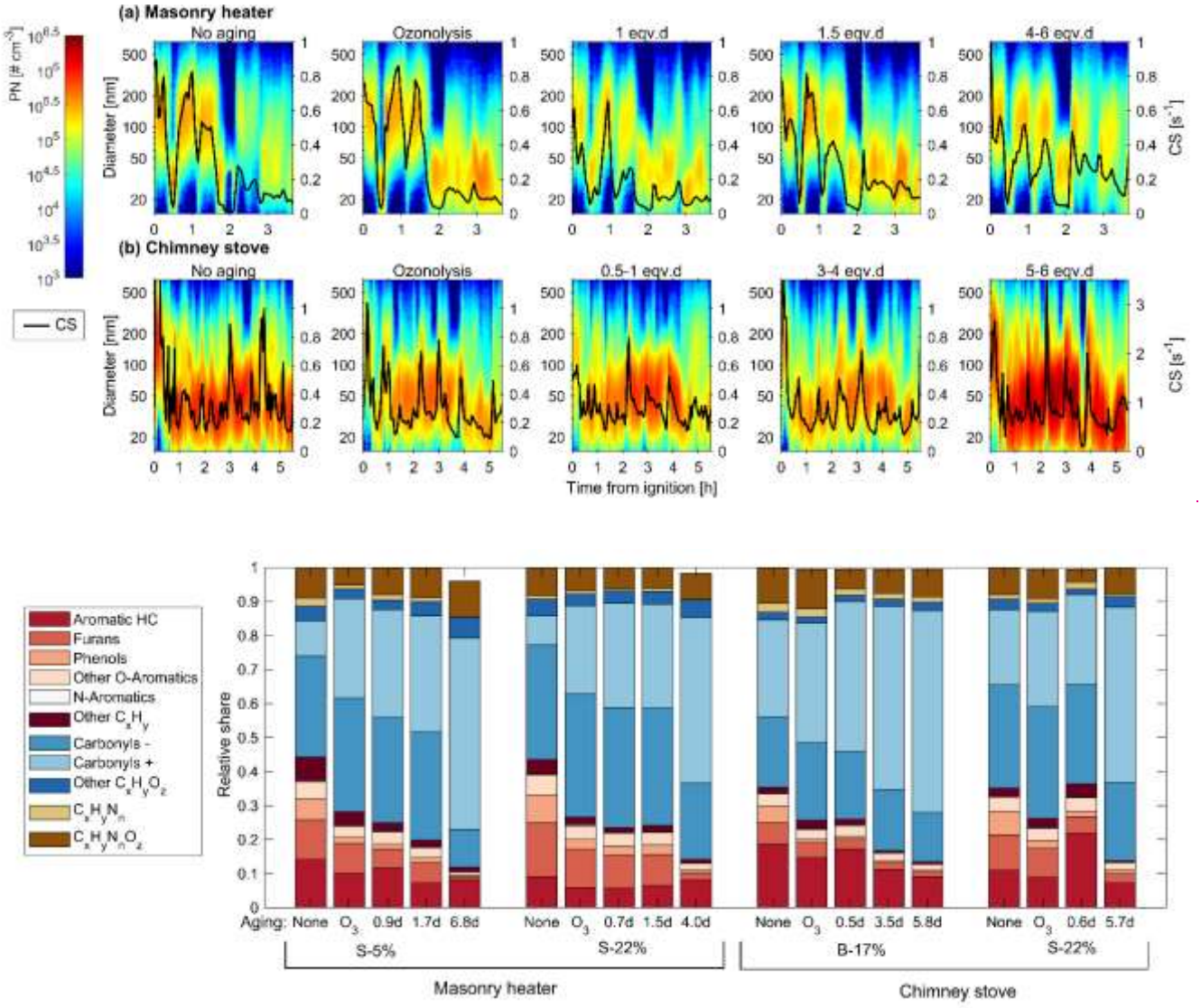

Figure 4: ~~Size distributions of diluted primary aerosol entering the oxidation flow reactor as a function of time, and condensation sinks (CS) in the PEAR based on average of size distributions before and after PEAR.~~

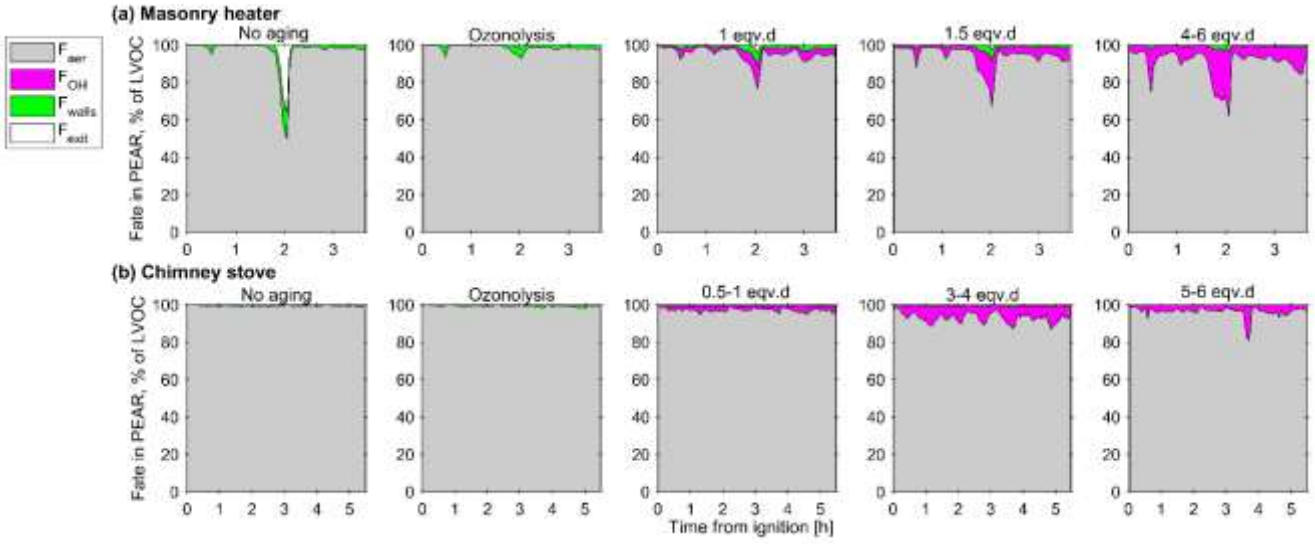

1060

~~Figure 5: Estimated fates of the low-volatility organic compounds in the PEAR during the experiments with portions of the LVOCs condensing onto particles (F_{aer}) and walls (F_{walls}) and lost in reactions with OH (F_{OH}). The remainder of the LVOCs (F_{exit}) exit the PEAR as LVOCs.~~

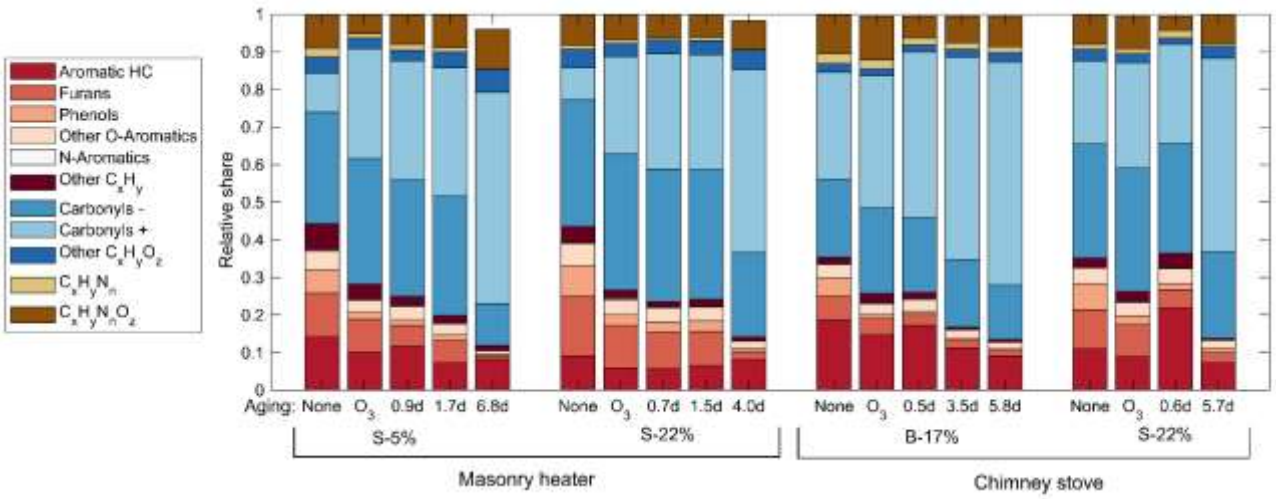

1065 **~~Figure 6:~~ Relative shares of the ~~identified VOC~~OGC groups in the exhaust ~~after~~downstream the PEAR OFR as measured by PTR-ToF-MS, averaged over the total experiment time covering 2–5 batches.**

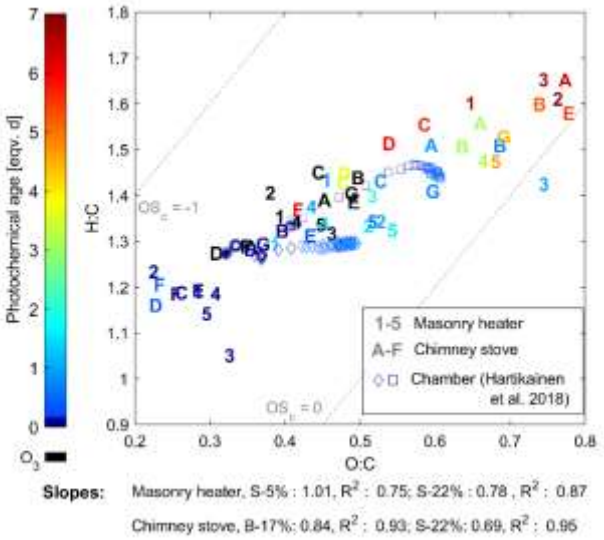

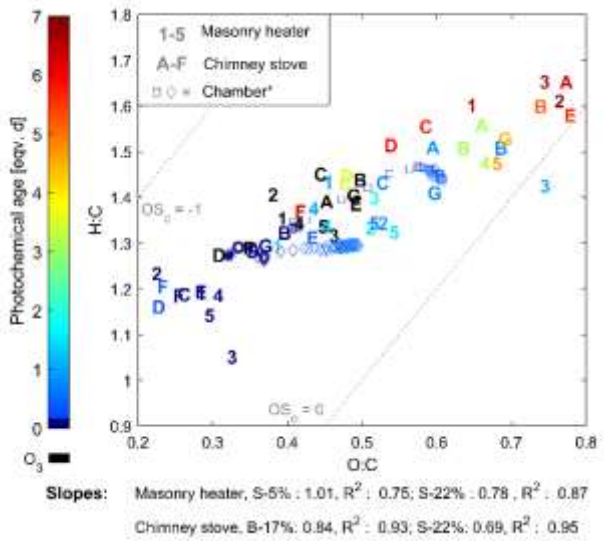

Figure ~~75~~: Van Krevelen diagram of the ~~VOCs~~OGCs measured ~~with~~by PTR-ToF-MS. Numbers indicate batches combusted in masonry heater (1–3 dry spruce, 4–5 moist spruce); letters refer to chimney stove batches (A–E beech, F–G moist spruce). Ozonolysis experiments (in black) were not considered in the slope calculations. *Behaviour of RWC emission aged in a chamber (Hartikainen et al., 2018) ~~is marked with scatter.~~

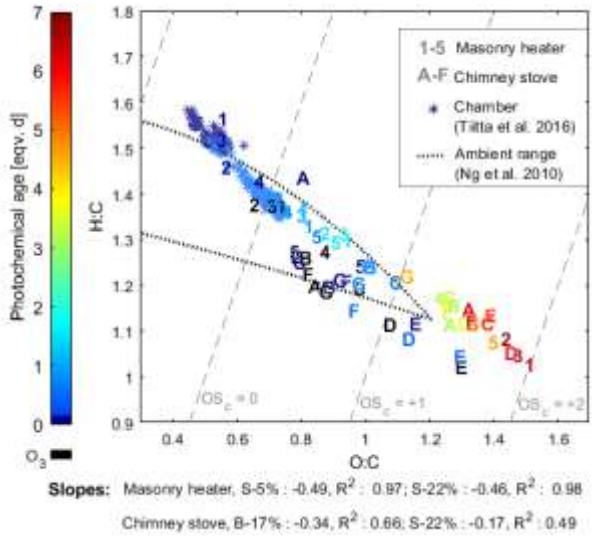

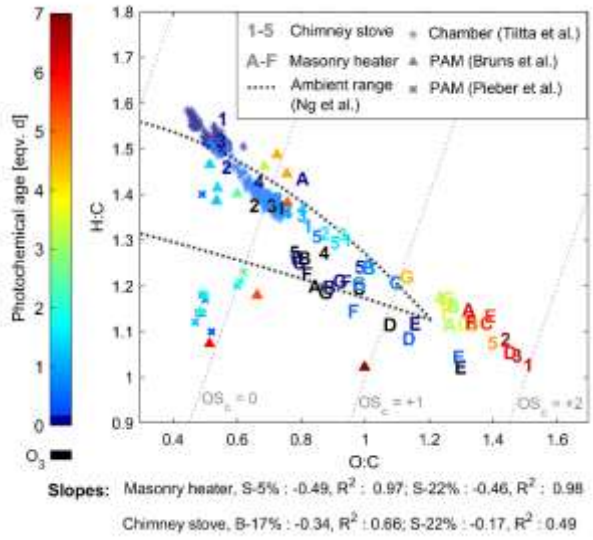

Figure ~~86~~: Van Krevelen diagram of the particulate organic aerosol measured by SP-HR-ToF-AMS. Numbers indicate batches combusted in masonry heater (1–3 dry spruce, 4–5 moist spruce), whereas letters refer to chimney stove batches (A–E beech, F–G moist spruce~~).~~) of this study. Ozonolysis experiments are marked with black and were not considered in slope calculations. ~~The~~Results from aging of RWC exhaust with a PAM OFR by Bruns et al. (2015a) and Pieber et al. (2018), as well as behaviour of RWC OA aged in a chamber (Tiitta et al., 2016) ~~with slopes of -0.64 to -0.67 is~~are marked with scatter.

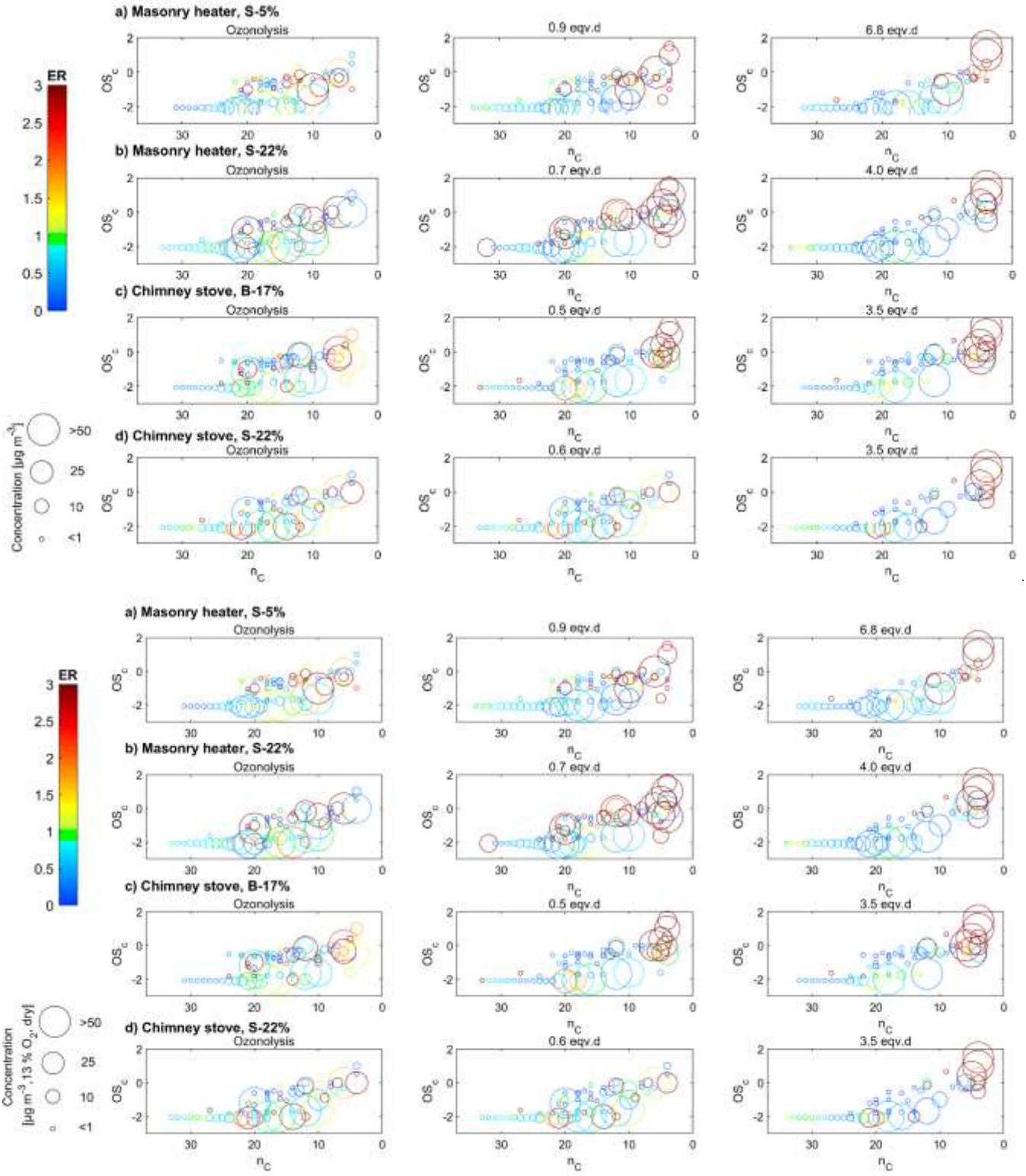

Figure ~~9~~7: Compounds measured by IDTD-GC-ToFMS in different experiments (ozonolysis, low, and high photochemical exposure) with respect to their carbon number (n_C) and oxidation state (OS_C). Enhancement ratios (ER) compared to the experiments without oxidative aging are shown in colour, and the size indicates the dilution-corrected concentrations (normalised dry, 13% O_2 flue gas conditions) in the secondary exhaust.

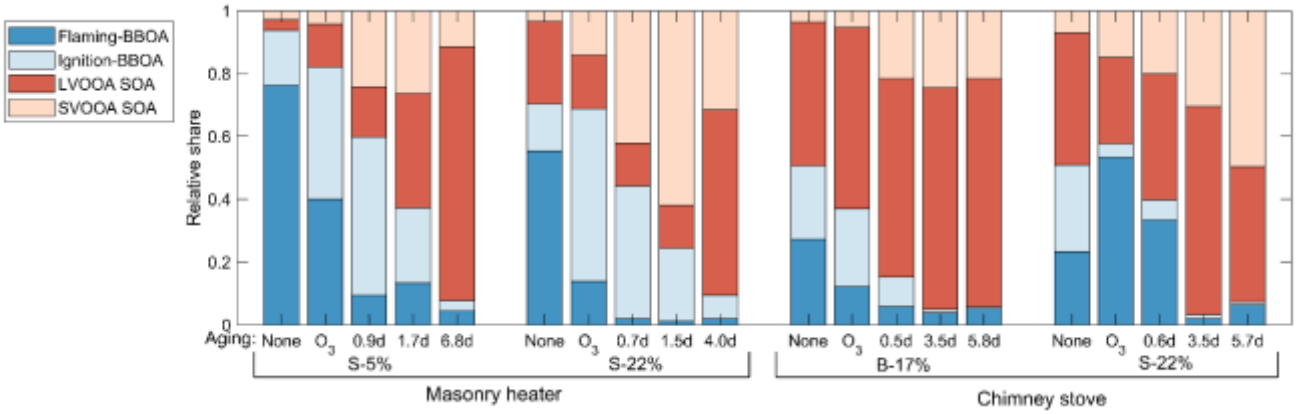

Figure ~~108~~: Average shares of the four PMF factors in the exhaust ~~after the PEAR at the~~at different exposure levels.

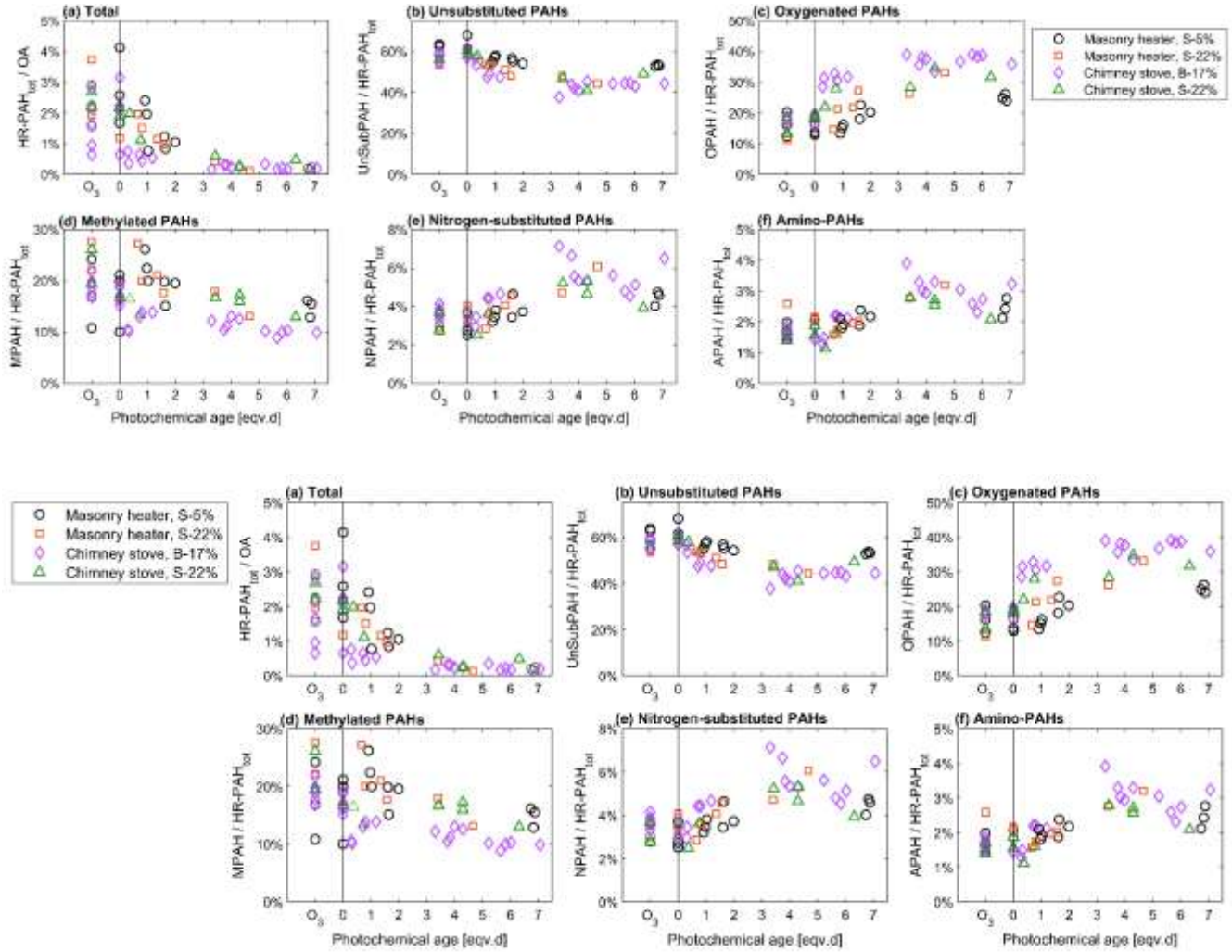

Figure ~~119~~: Relationship of photochemical aging to the batchwise average ratios of~~:~~ (a) total HR-PAH concentration to OA concentration ~~measured by AMS,~~ and (b–f) of HR-PAH subgroups to the total PAC concentration, measured by the SP-HR-ToF-AMS.

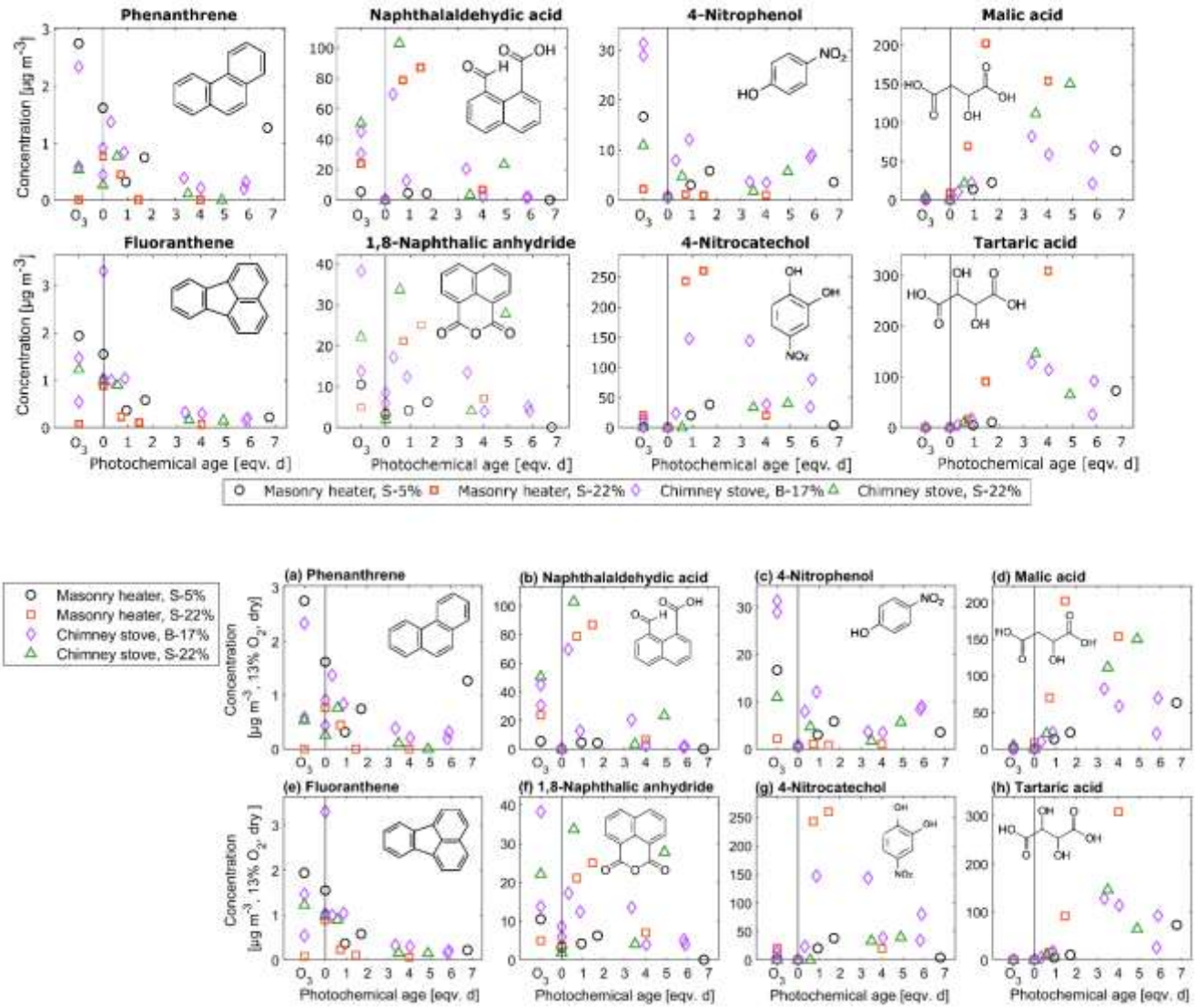

Figure ~~12: Concentrations of~~10: Dilution corrected concentrations for selected compounds measured by IDTD-GC-ToFMS at different exposure levels. Normalised to dry, 13% O_2 flue gas conditions.